NASA Contractor Report 179473
UC-MIE-051586-19

IN-14870

Dynamic Loading on Parallel Shaft Gears

Hsiang-Hsi (Edward) Lin
Memphis State University
Memphis Tennessee

and

Ronald L. Huston
University of Cincinnati
Cincinnati, Ohio

July 1986

Prepared for
Lewis Research Center
Under Grant NSG-3188

National Aeronautics and
Space Administration

TABLE OF CONTENTS

I. INTRODUCTION

I.1 Preliminary Remarks

This report presents a computer-based method of analysis of spur gear system dynamics. The report is based upon research conducted by the authors at the University of Cincinnati with the support of the NASA Lewis Research Center from 1982 to 1985 under Grant NSG 3188. The report represents a portion of the first author's doctoral dissertation.

Knowledge of the dynamic effects in gear systems has been of increasing interest--stimulated by demands for stronger, higher-speed, improved-performance, and longer-lived systems. There have been numerous research efforts directed toward gear dynamic analysis. Still, the basic behavior of the gear system has not been satisfactorily understood.

For example, in industrial settings, a high performance gear system is often obtained by overdesigning at the sacrifice of cost, material, and compactness. In aerospace or military applications, where weight is a premium, geared systems are often designed under conditions very close to the failure limits, thus introducing uncertainties in performance and life prediction. Moreover, gear systems are generally designed using static analyses. However, when gear systems are operating at high-speed, there are several factors affecting their performance which are enhanced by the speed. Specifically, the gear behavior can be affected by such items as:

1) Torsional stiffness of the gear shafts.
2) Gear tooth loading and deflection.
3) Gear tooth spacing and profile errors
4) Speed of the rotating bodies.

5) Mounting alignment.

6) Dynamic balance of rotating elements.

7) The mass of the gears and shafts.

8. The mass of the driving (power) and driven (load) elements.

There is not full agreement by researchers on the best methods for evaluating dynamic load effects. Hence, a gear designer is often confronted with conflicting theories. Therefore designers have had to rely on past experience, service safety factors, and upon experimental data with limited range of applicability.

If major advances in mechanical reliability, optimum performance and design automation are to be obtained, more in-depth understanding of the dynamic behavior is needed. Computer analysis and experimental investigation are two suitable approaches for this study. Experiments which produce reliable results are costly involving time consuming procedures. Experiments are generally more expensive, both in time and money, than computer analysis. Hence, if reliable computer software can be developed, taking into account the parameters used in experiments, many experimental hours in the analysis and design of spur gear systems could be saved.

I.2 Literature Survey

Research efforts on gear system dynamics have been conducted for many years. In 1892, Lewis [1]* recognized that the instantaneous load

*Numbers in brackets refer to References at the end of the Report.

of the tooth was affected by the velocity of the system. In 1925, a large experimental program was started by a research committee, headed by Earl Buckingham [3], and endorsed by the American Society of Mechanical Engineers. They published the first authoritative report on gear dynamics in 1931. This report presented a procedure on determining the so-called dynamic load increment due to mesh dynamics and gear tooth errors.

In 1959, Attia [4] performed experiment to determine actual instantaneous loading. He found that Buckingham's results gave more conservative values.

In 1958, Niemann and Retti [5] found that larger masses caused higher dynamic loads, but as the average load became larger the effect of larger masses became less important. They also found that very heavily loaded gear systems showed no appreciable dynamic load increment, whereas in lightly and moderately loaded gear systems there were considerable dynamic load increments. In 1958, Harris [6] suggested that for gear systems isolated from external stimuli, there are three internal sources of dynamic loads: 1) Error in the velocity ratio measured under the working load; 2) Parametric excitation due to stiffness variation of the gear teeth; and 3) Non-linearity of tooth stiffness when contact is lost. In 1970, Houser and Seireg [7] developed a generalized dynamic factor formula for spur and helical gears operating away from system resonances. The formula took into consideration the gear geometry and manufacturing parameters as well as the dynamic characteristics of the system.

In 1972, Ichimaru and Hirano [8] analyzed heavy-loaded spur gear systems with manufacturing errors under different operating conditions. They found that the change in tooth profile showed a characteristic trend to decrease dynamic load. In 1978, Cornell and Westervelt [9]

presented a closed form solution for a dynamic model of spur gear system and showed that tooth profile modification, system inertia and damping, and system critical speeds, can have significant effect upon the dynamic loads. In 1981, Kasuba and Evans [10] presented a large scale digitized extended gear modeling procedure to analyze spur gear systems for both static and dynamic conditions. Their results indicated that gear mesh stiffness is probably the key element in the analysis of gear train dynamics. They showed that the gears and the adjacent drive and load systems can be designed for optimum performance in terms of minimum allowable dynamic loads, for a wide range of operating speeds.

In 1981, Wang and Cheng [11] developed another dynamic load response algorithm. They reported that the dynamic load is highly dependent on the operating speed. Nagaya and Uematsu [12] stated that because the contact point moves along the involute profile, the dynamic response should be considered as a function of both the position and speed of the moving load. In 1982, Terauchi, et al. [13] studied the effect of tooth profile modifications on the dynamic load of spur gear systems. According to their results, the dynamic load clearly decreased with proper profile modifications.

I.3 Objective

The objective of the research reported herein is the development of a theoretical basis and an associated comptuer-aided design procedure, for studying dynamic behavior of spur gear systems. Procedures for the research include the following steps:

1. The development of a mathematical model of spur gear systems consisting of the gears, the shafts, and the connected masses.
2. The evaluation of the properties of the system components.
3. The development of governing equations for the entire system.
4. The development of a static and dynamic analyses of the system.
5. An examination of the effects upon system behavior of the following parameters:

    Mass moments of inertia

    Stiffness of components

    Operating speeds of system

    Damping factors

    System Natural Frequency

    Contact ratios

6. The development of system component modification for design optimization.

The computer software developed herein is intended to be used by engineer and designers in the development of actual gear systems. The developed software is believed to be among the most detailed and advanced prepared to date.

II. THE SYSTEM AND ITS PROPERTIES

II.1 System Definition and Methods of Analysis

Figure II.1 shows a sketch and a schematic model of NASA 3000-hp transmission stand. The system is very elaborate. However, one can view the system as containing three basic elements: The first is the gear; the second is the shaft; and the third is the mass connected to the shaft. Hence, an elaborate system can be modelled by components consisting of simple gear set. Figure II.2 illustrates a model of a simple spur gear system with those three basic elements.

The system properties such as stiffness, inertias, dampings, frictions, contact ratio, need to be determined to develop the dynamic analysis.

The static properties of the system and its components may be obtained from the literature in gearing, and from the principles of strength of materials, mathematics, lubrication, vibration analysis, and finite element methods. These properties are useful in the sequel in conducting the dynamic analysis.

Given the model, the governing equations of the system are written and integrated. It is assumed that the dynamic activity of the gears is confined to the rotating plane of the gears. The rotating axes are assumed to be symmetrical. Out-of-plane twisting and misalignment effects are neglected.

A parametric study is performed to examine the relative effects of rotating speed, applied load, lubrication and damping, mass, stiffness, diametral pitch and contact ratio.

Finally, analaytical procedures are developed for computer-aided design of the system. Specifically, the system is modified to obtain

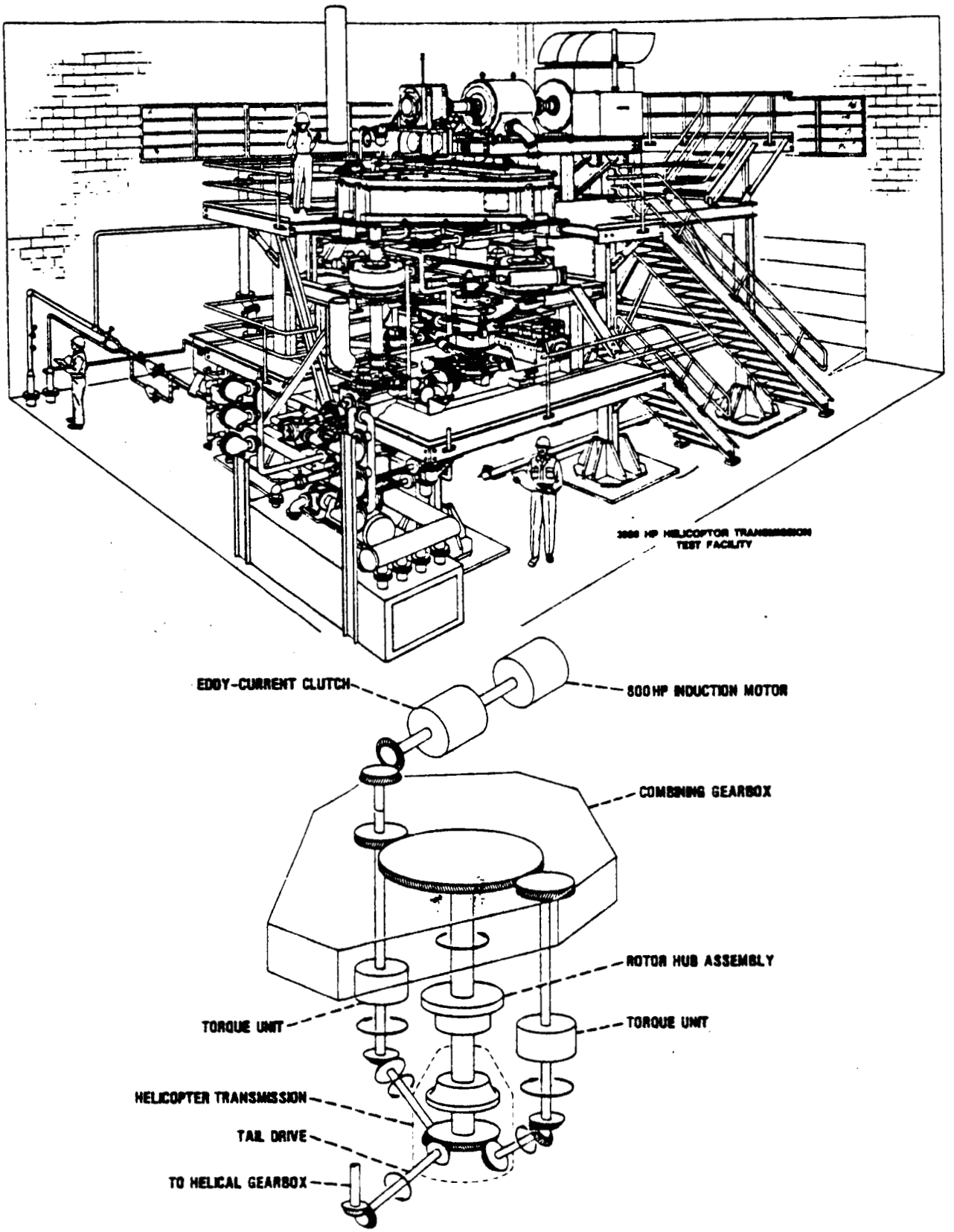

Figure II.1 NASA Lewis Research Center's 3000-hp Helicopter Transmission Test Stand and Schematic Arrangement.

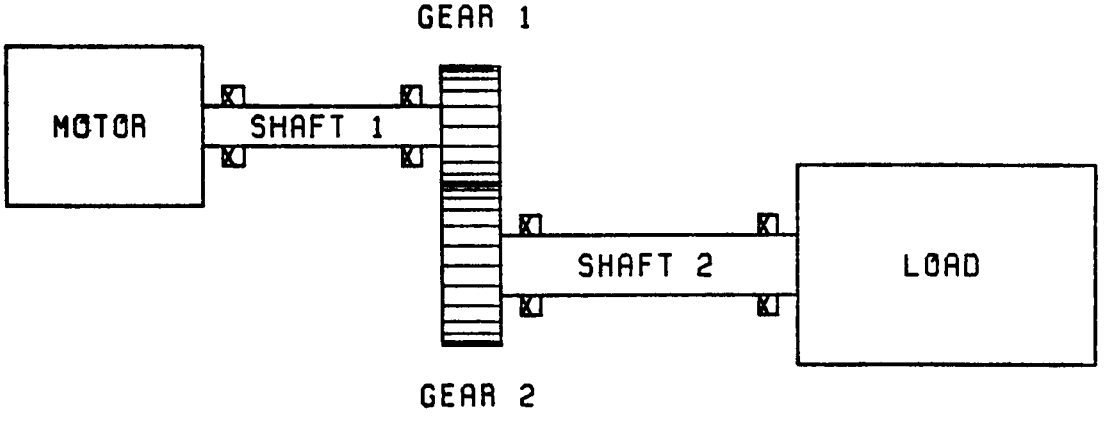

Figure II.2. A Simple Spur Gear System Model

improved performance based upon the results of the simulation. These are discussed in a subsequent report.

II.2 Spur Gear Geometry: The Involute Curve and Its Use as a Tooth Profile

The Involute curve is used almost exclusively for spur gear tooth profiles. The involute provides numerous kinematic advantages. The involue generally described as the curve generated by the locus of the end of a line unwound from the circumference of a circle. See Figure II.3. The circle from which the string is unwound is called the "base circle."

The equations of the involute may be developed as follows: Let R_b be the radius of base circle. Let r and θ be the radial and angular coordinates of a point on the involute, and let β be the angle displaced by the tangent line as shown in Figure II.3. Hence, we have

$$\theta = \beta - \psi = \beta - \tan^{-1} \frac{\sqrt{r^2 - R_b^2}}{R_b} \qquad (II.1)$$

where ψ is the difference between β and θ as shown.

The length of the generating line $\sqrt{r^2 - R^2_b}$ is also the length of the circumference of the base circle subtended by the angle β. Hence, we have

$$\sqrt{r^2 - R^2_b} = R_b \beta \quad \text{or} \quad \beta = \frac{\sqrt{r^2 - R_b^2}}{R_b} \qquad (II.2)$$

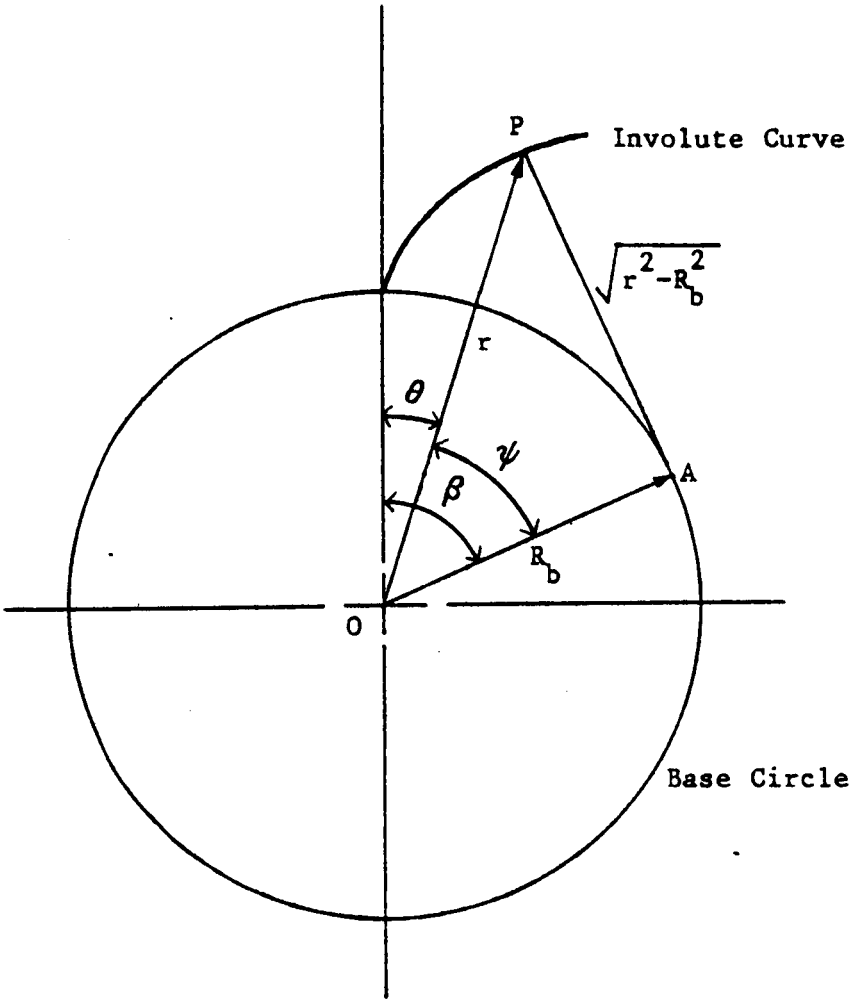

Figure II.3 Involute Curve Geometry

Then from Equation (II.1) we have

$$\theta = \frac{\sqrt{r^2 - R_b^2}}{R_b} \qquad \tan^{-1} \frac{\sqrt{r^2 - R_b^2}}{R_b} \tag{II.3}$$

This is the polar representation of the involute curve. The generating line is always normal to the involute curve and its length is a measure of the radius of curvature of the involute curve. For example, length AP is the radius of curvature of involute curve at point P.

Consider the action of one involute against another involute as shown in Figure II.4. The point of contact between the two involutes is that point where the tangents to the two curves coincide. The tangents to both involutes are always perpendicular to their generating lines. Hence, the tangents to the two involutes coincide only when the generating line of one is a continuation of the generating line of the other. Therefore, the locus of points of contact between two involutes is the common tangent (AB) to the two base circles as shown in Figure II.4.

When an involute is revolved at a uniform rate, the length of its generating line (AE) changes uniformly. Similarly, the length of the generating line (BD) on the mating involute changes at the same uniform rate. The length of the common tangent (AB) to the two base circles remains constant. Hence, the relative rate of motion depends only upon the relative sizes of two base circles. The contact takes place only along the common tangent. The relative rates of rotation are independent of the distance between the centers of the two base circles.

The relative rates of rotation of the two involutes may be represented by two plain disks which drive each other by friction. Such disks are known as pitch disks, while their diameters are known as pitch diameters.

From Figure II.4 we see that the intersection of the common tangent (AB) with the common center line (O_1O_2) of the two involutes establishes the pitch point P and the radii of the two pitch circles: R_{p1} and R_{p2}.

The angle between this common center line O_1O_2 and a line perpendicular to the common tangent AB is called the pressure angle. There is a relation between the pitch diameter, base diameter, and pressure angle of any given involute. That is for a given pitch diameter, there is a unique corresponding pressure angle: Let R_{b1} and R_{b2} be the base radii and let R_{p1} and R_{p2} be the pitch radii of first and second involutes.

Let ϕ be the pressure angle.

Then

$$R_{b1} = R_{p1} \cos\phi \quad \text{and} \quad R_{b2} = R_{p2} \cos\phi \tag{II.4}$$

Next, consider Figure II.5 which shows the involute profile change with roll angle. Let ε represent the roll angle, and let the angular intervals ε_b, ε_c, ε_d, and ε_e be equal. We note from Figure II.5 that the length of the curve ab is much less than that of bc; that bc is shorter than cd; etc. Thus, when two involutes are acting against each other, a combined rolling and sliding action takes place due to the varying lengths of equal angular increments on the profiles. From Figure II.5 it is evident that the rate of sliding between two involutes is continually varying. The sliding which is high initially reduces to

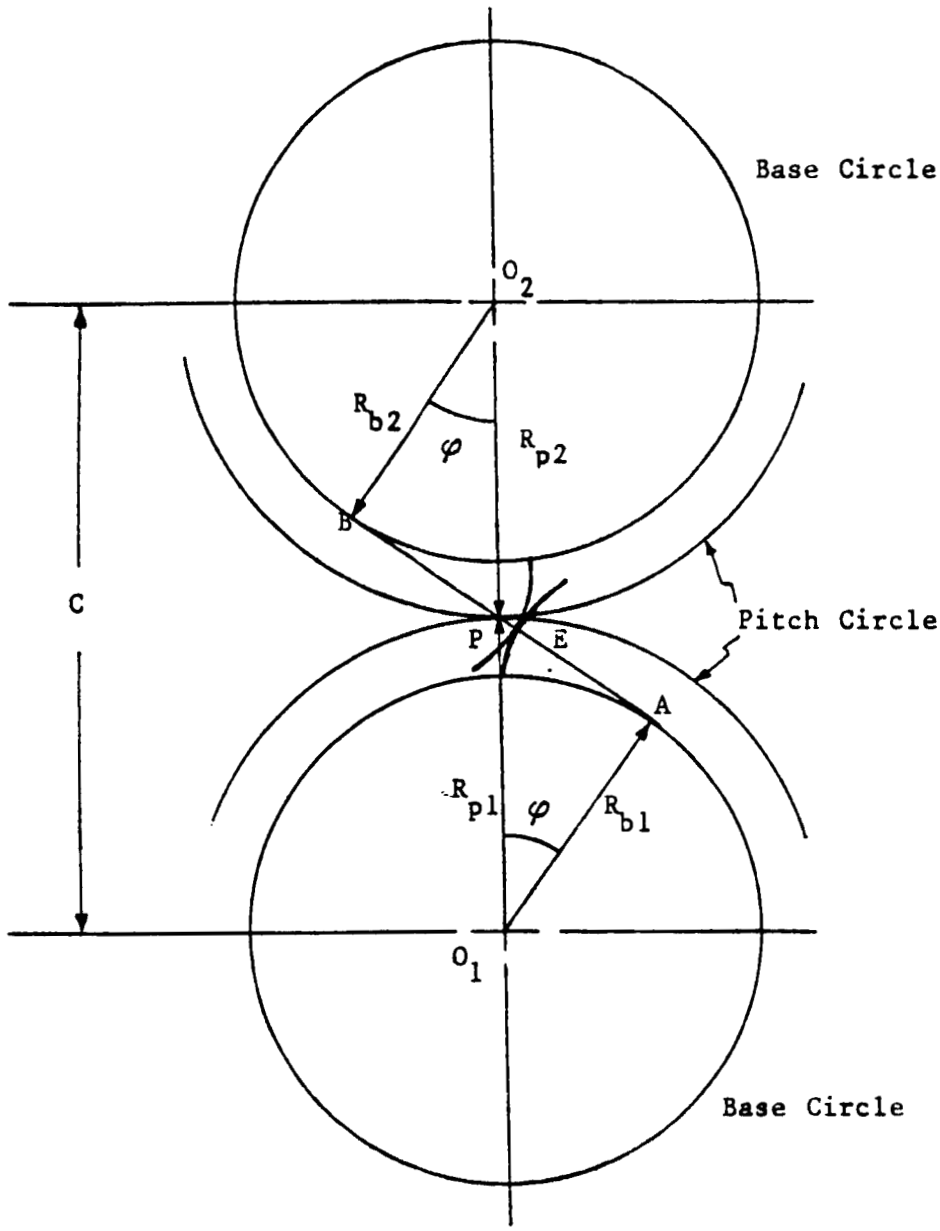

Figure II.4 Action of One Involute Against Another

zero at the pitch point, and then changes direction, and increases again.

Equations for determining the sliding speed at any point on a pair of involute gear teeth may be derived as follows [1]: The sliding speed is the difference in speeds of the ends of the generating lines of the involutes, projected normal to the line of action, as they pass through the line of action. The angular velocity of these generating lines is the same as the angular velocities of the gears themselves. The sliding speed is then determined from the products of the angular velocities and the lengths of the generating lines.

Hence from Figure II.6 the sliding speed V_s may be expressed as:

$$V_s = (R_{c1}\omega_1 - R_{c2}\omega_2) \qquad (II.5)$$

where R_{c1} and R_{c2} are the tooth radii of curvature of the driving and driven gears and where ω_1 and ω_2 are the angular speeds of the driving and driven gears. Let V be the pitchline speed. Then V may be expressed as

$$V = R_{p1}\omega_1 = R_{p2}\omega_2 \qquad (II.6)$$

where R_{p1} and R_{p2} are the pitch radii of the driving and driven gears. Hence, by substituting for ω_1 and ω_2 in Equation (II.5) the sliding speed becomes:

$$V_s = V\left(\frac{R_{c1}}{R_{p1}} - \frac{R_{c2}}{R_{p2}}\right) = V\left(\frac{R_{p2}R_{c1} - R_{p1}R_{c2}}{R_{p1}R_{p2}}\right) \qquad (II.7)$$

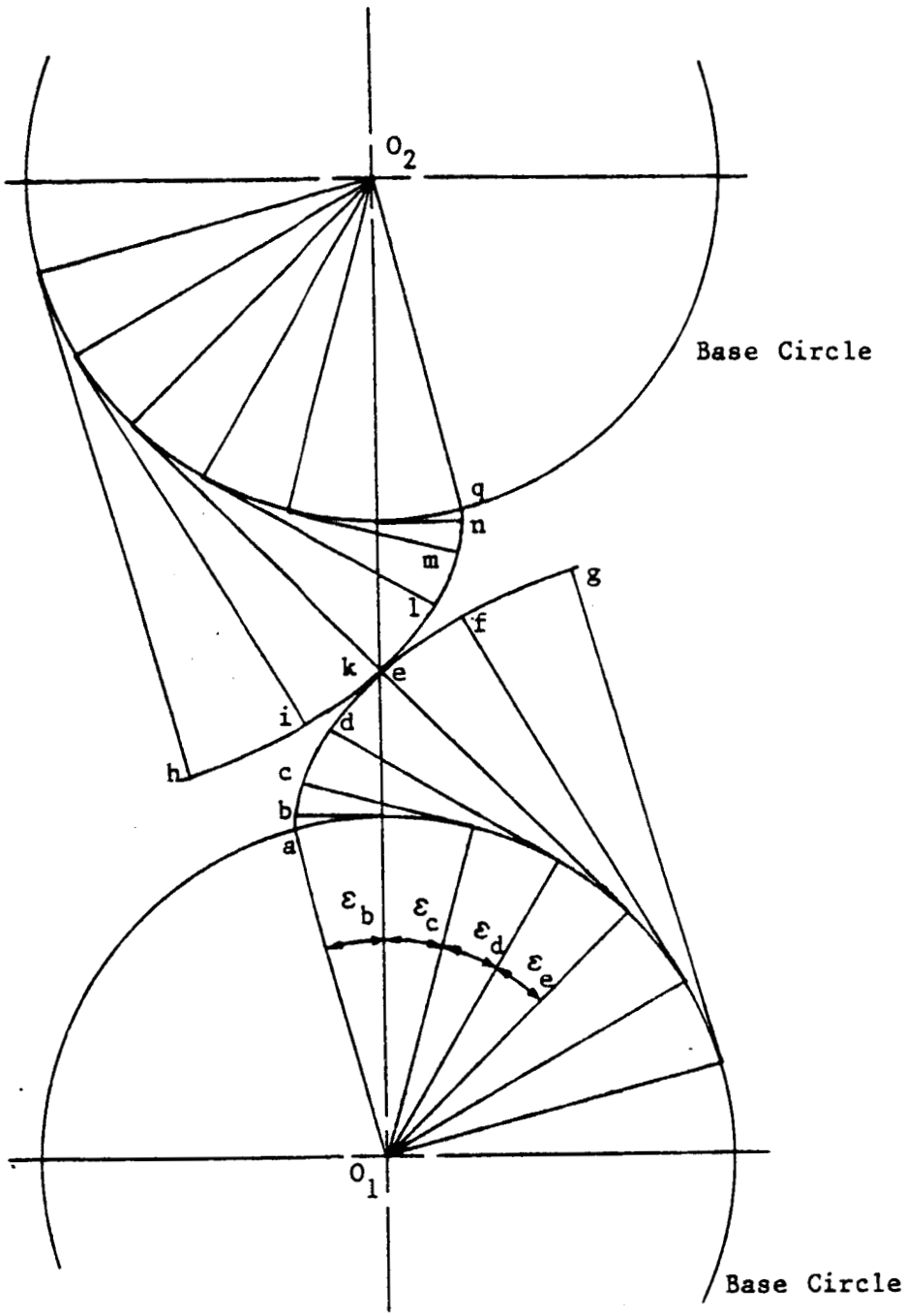

Figure II.5 Roll Angle and Change of Involute Profile Length

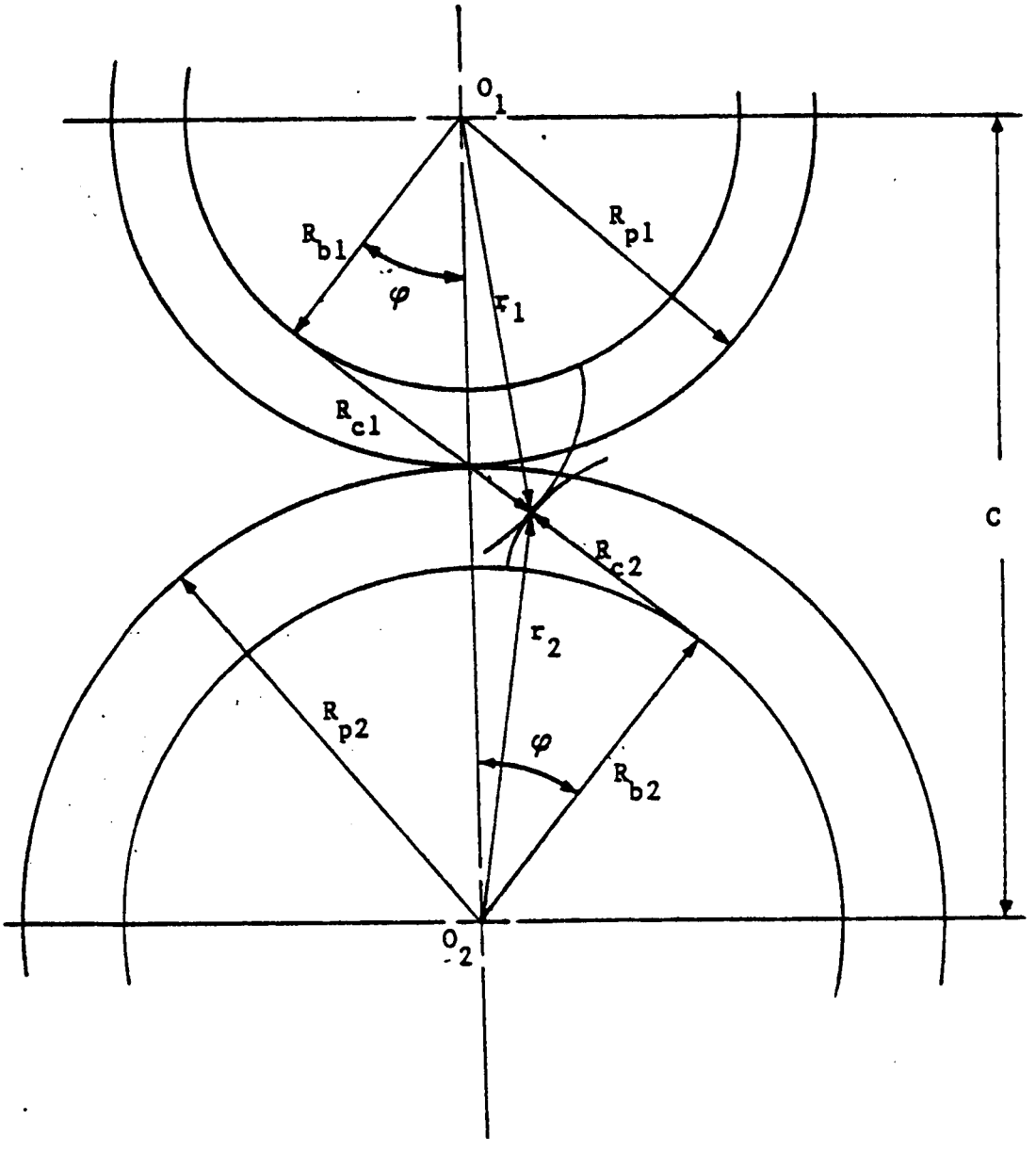

Figure II.6 Involute Tooth Profile for Determining Sliding Velocity.

Next, let r_1 and r_2 measure the radial distance from the gear centers to the tooth contact point as shown in Figure II.6. Then R_{e1} and R_{e2} may be expressed in terms of r_1, r_2, the pressure and ϕ, the base circle radii R_{b1} and R_{b2} and the pitch radii as:

$$R_{c1} + R_{c2} = (R_{p1} + R_{p2}) \sin\phi \tag{II.8}$$

and

$$R_{c1} = \sqrt{r_1^2 - R_{b1}^2} \tag{II.9}$$

and

$$R_{c2} = \sqrt{r_2^2 - R_{b2}^2} = (R_{p1} + R_{p2})\sin\phi - \sqrt{r_1^2 - R_{b1}^2} \tag{II.10}$$

Finally, by substituting for R_{c1} and R_{c2} in Equation (II.7) the sliding speed V_s becomes (see [1]):

$$V_s = \frac{V}{R_{p1}R_{p2}} \left\{ R_{p2}\sqrt{r_1^2 - R_{b1}^2} - R_{p1}\left[(R_{p1}+R_{p2})\sin\phi - \sqrt{r_1^2 - R_{b1}^2}\right] \right.$$
$$\left. = \frac{V}{R_{p1}R_{p2}} (R_{p1}+R_{p2}) \left[\sqrt{r_1^2 - R_{b1}^2} - R_{p1}\sin\phi\right] \right\} \tag{II.11}$$

II.3 Deflection and Stiffness of Spur Gear Teeth

The static deflection of a pair of mating teeth is assumed to be composed of the following components:

1. Cantilever beam deflection of gear teeth including bending, shear, and compression deformation.
2. Deflection due to rotation of tooth base because of the flexibility of tooth foundation.
3. Local contact (Hertz) deformation at contact point.

The deflection of a gear tooth is calculated normal to the tooth profile. The foundation effect and the shear effect are important because of the "stubbiness" of a gear tooth. In this research phase we consider only Low Contact Ratio Gears (LCRG), with contact ratio between 1.0 and 2.0. However, the analysis can easily be extended to higher contact ratio gears.

II.3.1 Direction of the Applied Load on a Tooth Profile

The application point and direction of the transmitted load by meshing teeth at different contact positions can be obtained through the involutometry of the tooth profile: given the pitch radius R_p, the pressure angle ϕ, and the circular pitch P_c, let an X-Y coordinate system be defined as shown in Figure II.7. The tooth thickness on the pitch circle, t_p, is approximately half of the circular pitch P_c. The tooth thickness t_i at any other point i on the tooth profile, with radius R_i from the gear center, can be expressed as

$$t_i = 2 R_i [(t_p/2R_p) + \text{inv}\phi - \text{inv}\theta_i] \qquad \text{(II.12)}$$

where $\theta_i = \cos^{-1}(R_b/R_i)$ and where inv x is the involute function defined as:

$$\text{inv } x = \tan x - x \qquad \text{(II.13)}$$

The angle x between the Y-axis and the radial line to the contact point is:

$$\psi_i = (t_p/2R_p) + \text{inv}\phi - \text{inv}\theta_i \qquad \text{(II.14)}$$

The angle β between the transmitted load at point i and the x-axis is:

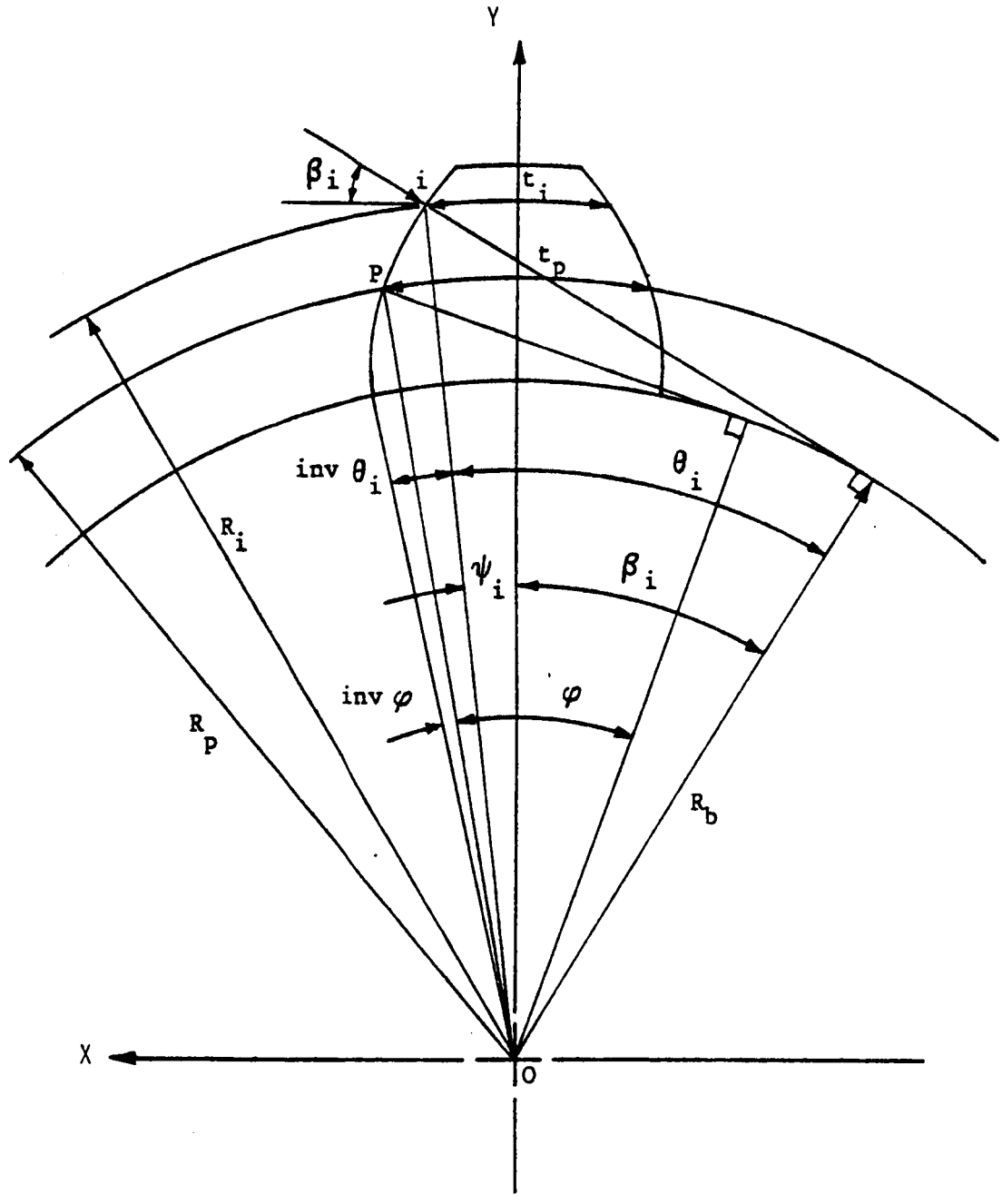

Figure II.7 Direction of Transmitted Load

$$\beta_i = \theta_i - \psi_i \tag{II.15}$$

The chordal tooth thickness h at point i is

$$h_i = 2R_i \sin\psi_i \tag{II.16}$$

Finally, the x and y coordinates at point i are:

$$\begin{aligned} Y_i &= R_i \sin\psi_i \\ X_i &= R_i \cos\psi_i \end{aligned} \tag{II.17}$$

These coordinates will be useful in developing geometrical properties for calculating deflection and stiffness.

II.3.2 The Tooth As a Cantilever Beam

The involute portion of a gear rooth may be modelled as a non-uniform cantilever beam [9, 14]. Let $\bar{\ell}_o$ be an effective length which extends from the tip to the beginning of fillet area as shown in Figure II.8. Let the beam be divided into a sequence of segments as shown. The deflection and compliance can then be obtained using the principles of elementary strength of materials. For each segment i, the height $\bar{Y}_i$, the cross-sectional area $\bar{A}_i$, and the area moment on inertia $\bar{I}_i$ are taken as average values at both faces according to the equations:

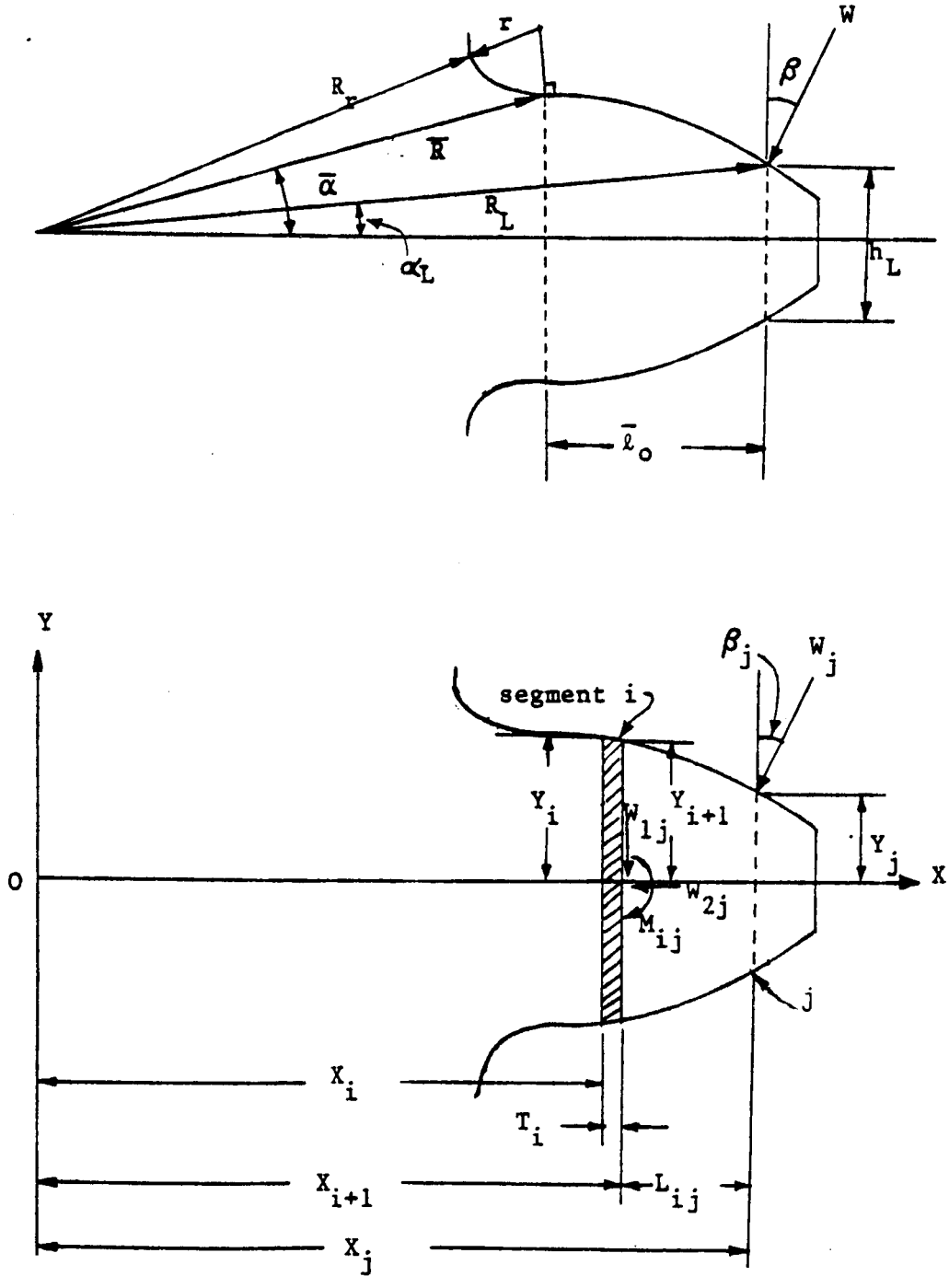

Figure II.8 Geometry and Segment Modelling of the Involute Portion

$$\bar{Y}_i = (Y_i + Y_{i+1}) / 2$$
$$\bar{A}_i = (A_i + A_{i+1}) / 2 = 2 F Y_i \qquad \text{(II.18)}$$
$$\bar{I}_i = (I_i + I_{i+1}) / 2 = F(Y_i^3 + Y_{i+1}^3)/3$$

where F is the face width. The deflection at the loading point, in the direction of load, is obtained by superimposing the deflection contribution of the individual segments. Each segment itself is considered as a cantilever beam having the inner end fixed and the remainder of the tooth adjacent to the other end of the segment, as a rigid overhand. Figure II.8 shows the applied load resolved into an equivalent system of forces and moments at the outer face of the segment. The components are:

$$W_{1j} = W_j \cos\beta_j$$
$$W_{2j} = W_j \sin\beta_j \qquad \text{(II.19)}$$
$$M_{ij} = W_j (L_{ij} \cos\beta_j - Y_j \sin\beta_j)$$

where i refers to the segment, j refers to the loading position, L_{ij} is the distance from j to i, W_j is the transmitted load, W_{1j} and W_{2j} are the component loads at i, and M_{ij} is the moment at i due to the load at j.

II.3.2.1 Bending deformation

The deformation at the load position j due to the deformation of segment i is the sum of the following:

(i) Displacements due to load $W_j \cos\beta_i$

$$(q_{B1})_{ij} = \frac{W_j \cos\beta_j}{3E_e \bar{I}_i} (T_i^3) \qquad \text{(II.20)}$$

$$(q_{R1})_{ij} = \frac{W_j \cos\beta_j}{2E_e \bar{I}_i} (T_i^2 \; L_{ij}) \qquad \text{(II.21)}$$

(ii) Displacements due to moments M_{ij}

$$(q_{B2})_{ij} = \frac{W_j (L_{ij} \cos\beta_j - Y_j \sin\beta_j)}{2E_e \bar{I}_i} (T_i^2) \qquad \text{(II.22)}$$

$$(q_{R2})_{ij} = \frac{W_j (L_{ij} \cos\beta_j - Y_j \sin\beta_j)}{E_e \bar{I}_i} (T_i L_{ij}) \qquad \text{(II.23)}$$

where T_i is the thickness of segment i, q_B is the displacement due to bending and q_R is the displacement due to rotation.

In the above expressions, E_e is the "Effective Young's modulus of elasticity" whose value depends upon whether the tooth is "wide" or "narrow". According to Cornell [14], a wide tooth is one for which

$$F/Y > 5 \qquad \text{(II.24)}$$

where Y is the tooth thickness at the pitch point. In this case the tooth approximates plain strain deformation and E_e is

$$E_e = E/(1 - \nu^2) \qquad \text{(II.25)}$$

where E is Young's modulus of elasticity and ν is Poisson's ratio. For a "narow" tooth,

$$F/Y < 5 \qquad \text{(II.26)}$$

In this case the tooth approximates plane stress deformation and E_e is:

$$E_e = E \qquad \text{(II.27)}$$

II.2.2.2 Shear Deformation

The shear deformation $(q_s)_{ij}$ is caused by the transverse component of the applied load. It displaces the centerline without rotation. For a rectangular cross section, the shear deformation is:

$$(q_s)_{ij} = \frac{1.2\ W_j T_i \cos\beta_j}{G\bar{A}_i} = \frac{2.4(1+\nu)\ W_j T_i \cos\beta_j}{E_e \bar{A}_i} \qquad (II.28)$$

II.2.2.3. Axial Compression

This axial compression $(q_c)_{ij}$ is caused by the component $W_j \sin\beta_j$ and is given by

$$(q_c)_{ij} = \frac{W_j \sin\beta_j T_i}{E\bar{A}_i} \qquad (II.29)$$

II.3.2.4 Totals

The total displacement at the load position j, in the direction of the load, due to deformation of segment i can thus be found from the expressions:

(1) For a wide tooth, (plane strain):

$$(q_1)_{ij} = (q_{B1}+q_{R1}+q_{B2}+q_{R2}+q_s)_{ij}\cos\beta_j + (q_c)_{ij}\sin\beta_j$$

$$= W_j \Big[\frac{\cos^2\beta_j}{E_e} \Big(\frac{T_i^3}{3\bar{I}_i} + \frac{T_i^2 L_{ij} + T_i L_{ij}^2}{\bar{I}_i}\Big) -$$

$$\frac{\cos\beta_j \sin\beta_j}{E_e} \Big(\frac{T_i^2 Y_j}{2\bar{I}_i} + \frac{T_i Y_j L_{ij}}{\bar{I}_i}\Big) +$$

$$\frac{\cos^2\beta_j}{E_e} \Big(\frac{2.4(1+\nu)T_i}{\bar{A}_i}\Big) + \frac{\sin^2\beta_j}{E_e} \Big(\frac{T_i}{\bar{A}_i}\Big)\Big] \qquad (II.30)$$

(2) For a narrow tooth (plane stress):

$$(q_1)_{ij} = W_j \frac{\cos^2\beta_j T_i}{E_e} \left[\frac{(T_i^3/3 + T_i L_{ij} + L_{ij}^2) - \tan\beta_j \left(\frac{T_j Y_j}{2} + Y_j L_{ij}\right)}{\bar{I}_i} + \frac{2.4(1+\nu) + \tan^2\beta_j}{\bar{A}_i}\right] \qquad (II.31)$$

II.3.3 Flexibility of the Fillet and Foundation

The effect of the flexibility of the foundation upon the deformation at the load point is a function of the fillet geometry, and the load position and direction. This deformation is influenced by the effective fillet length and the fillet angle (approximately 75°).

Figure II.9 shows a model of a gear tooth, its fillet, and its foundation. Using the notation of the figure, deflection in the direction of load at the loading point due to beam compliance of fillet region, q_{fb}, is given by the following expressions:

(1) For a narrow tooth (plane stress):

$$(q_{fb})_{ij} = W_j \left\{\frac{\cos^2\beta_j (T_{fb})_i}{E_e} \left[\frac{\frac{(T_{fb})_i^2}{3} + (T_{fb})_j (L_{fb})_{ij} + (L_{fb})_{ij}^2}{(\bar{I}_{fb})_i} - \frac{\tan\beta_j \left(\frac{(T_{fb})_i^2 Y_j}{2} + Y_j (L_{fb})_{ij}\right)}{(\bar{I}_{fb})_i} + \frac{2.4(1+\nu) + \tan^2\beta_j}{(\bar{A}_{fb})_i}\right]\right\} \qquad (II.32)$$

(2) For a wide tooth (plane strain):

$$(q_{fb})_{ij} = W_j \left\{\frac{\cos^2\beta_j}{E_e} \left[\frac{\frac{(T_{fb})_i^3}{3} + (T_{fb})_i^2 + (T_{fb})_i (L_{fb})_{ij}}{(\bar{I}_{fb})_i} + \frac{2.4(1+\nu)(T_{fb})_i}{(\bar{A}_{fb})_i}\right] - \frac{\cos\beta_j \sin\beta_j}{E_e} \left(\frac{\frac{(T_{fb})_i^2 Y_j}{2} + (T_{fb})_i Y_j (L_{fb})_{ij}}{(\bar{I}_{fb})_i}\right) + \frac{\sin^2\beta_j}{E_e} \left(\frac{(T_{fb})_i}{(\bar{A}_{fb})_i}\right)\right\} \qquad (II.33)$$

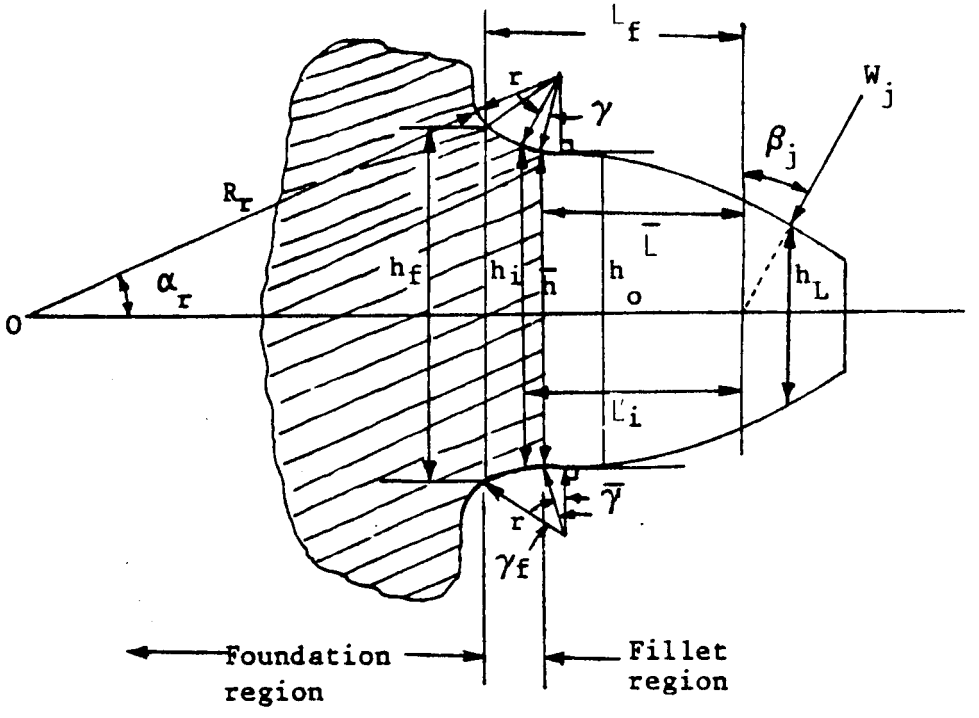

Figure II.9 Model of the Fillet and Foundation

Similarly, the deflection due to foundation flexibility, q_{fe} is:

(1) For narrow tooth (plane stress):

$$(q_{fe})_{ij} = \frac{W_j \cos^2\beta_j}{E_e F}\left[\frac{16.6}{\pi}\left(\frac{(L_f)_i}{h_f}\right)^2 + 2(1-\nu)\left(\frac{(L_f)_i}{h_f}\right) + 1.534\left(1 + \frac{\tan^2\beta_j}{2.4(1+\nu)}\right)\right] \quad \text{(II.34)}$$

(2) For a wide tooth (plane strain):

$$(q_{fe})_{ij} = \frac{W_j \cos^2\beta_j}{E_e F}(1-\nu^2)\left[\frac{16.67}{\pi}\left(\frac{(L_f)_i}{h_f}\right)^2 + 2\left(\frac{1-\nu-2\nu^2}{1-\nu^2}\right)\left(\frac{(L_f)_i}{h_f}\right) + 1.534\left(1 + \frac{\tan^2\beta_j}{2.4(1+\nu)}\right)\right] \quad \text{(II.35)}$$

where $(L_f)_i$ and h_f are

$$(L_f)_i = L_i + r(\sin\gamma_F - \sin\bar{\gamma}) \quad \text{(II.36)}$$

and

$$h_f = \bar{h} + 2r(\cos\bar{\gamma} - \cos\gamma_f) \quad \text{(II.37)}$$

where

$$L_i = (R_L)_i \cos(\alpha_L)_i - \frac{(h_L)_i \tan\beta_i}{2} - \bar{R}\cos\bar{\alpha} \quad \text{(II.38)}$$

A number of investigators have studied the flexibility of gear teeth. Experimental measurements have been made by Timoshenko and Baud [16], Walker [16], Buckingham [16], and Van Zandt [16]. Theoretical analyses have been developed by Timoshenko and Baud [16], Walker [16], Weber [16], Richardson [16], and Attia [16]. The results of some of these are compared with the results herein in Figure II.12. It is seen that they have similar shapes but different magnitudes. The discrepancy

may be due to the following factors:

1) Different reference points of zero deformation.

2) Different formulas used to calculate the deformation at the contact area.

3) Empirical formulas extended beyond the accuracies of experimental data.

Finally, the total deflection in the direction of load due to the flexibility of the fillet and the foundation is obtained by adding the above individual deflections. That is,

$$(q_2)_{ij} = (q_{fb})_{ij} + (q_{fe})_{ij} \tag{II.35}$$

II.3.4 Local Compliance Due to Contact Forces

The local contact deformation consists of two elements: One is the Hertz (or line-contact) deformation and the other is general compression of the tooth between the contact point and the tooth centerline.

Using procedures of Lundberg and Palmgren [37], for contact compliance of cylinders in roller bearing, the local deformation of gear teeth may be approximated as:

$$(q_3)_{ij} = \frac{1.275}{E12^{0.9} F^{0.8} W_j^{0.1}} \tag{II.37}$$

where

$$E12 = (2\ E1\ E2)/(E1 + E2) \tag{II.38}$$

where E1 and E2 are the elastic modulii of the driving and driven gears respectively. Equation (II.37) gives the contact compliance at the jth calculation point. However, the compliance depends upon the magnitude

of the load shared at the loading position. The magnitude is unknown. Nevertheless, since the load in Equation (II.37) is raised to the one-tenth power, there is little error in replacing it by the average transmitted load.

II.3.5 Total Deflection and Stiffness

The total deformation $(q_t)_j$ at load position j in the direction of load is the sum of all the deformations calculated above. If the number of segments is n, then

$$(q_t)_j = \sum_{i=1}^{n} [(q_1)_{ij} + (q_2)_{ij} + (q_3)_{ij}] \qquad (II.39)$$

Figures II.10 to II.12 show the normalized total deformation of a pair of teeth along path of contact for two different cases (different gear radii).

The equivalent stiffness of a gear tooth is defined as the ratio of the transmitted load and the total deformation:

$$(Kg)_j \overset{D}{=} W_j/(q_t)_j \qquad (II.40)$$

Hence the average stiffness of a meshing tooth pair is:

$$(Kg)_{avg} = \frac{1}{n} \sum_{i=1}^{n} (Kg)_j \qquad (II.41)$$

where n is the number of meshing positions.

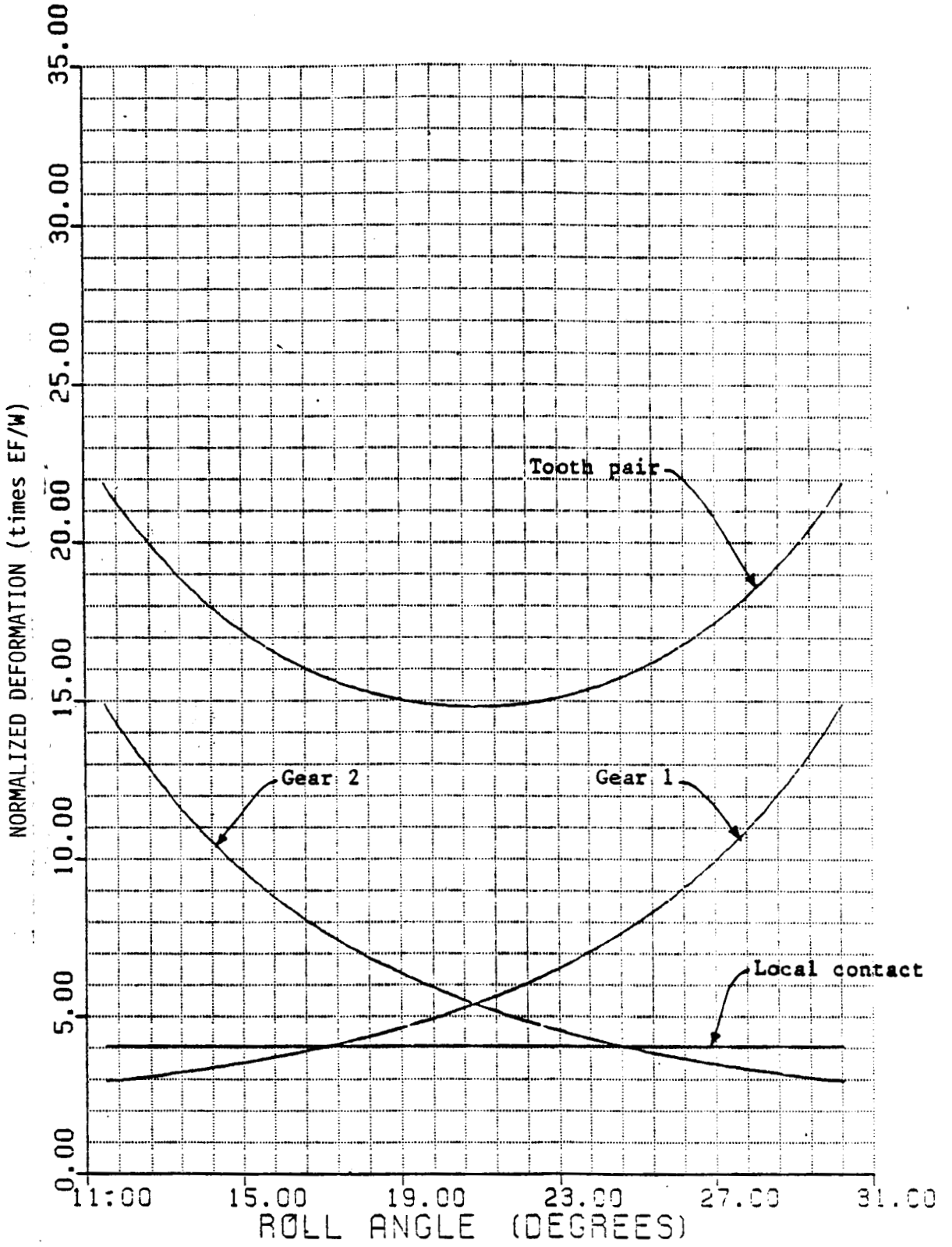

Figure II.10 Normalized Deformations of a Pair of Teeth, Diametral Pitch: 8; Pressure Angle: 20°; Pitch Radii: $R_{p1} = R_{p2} = 2.25$ in.

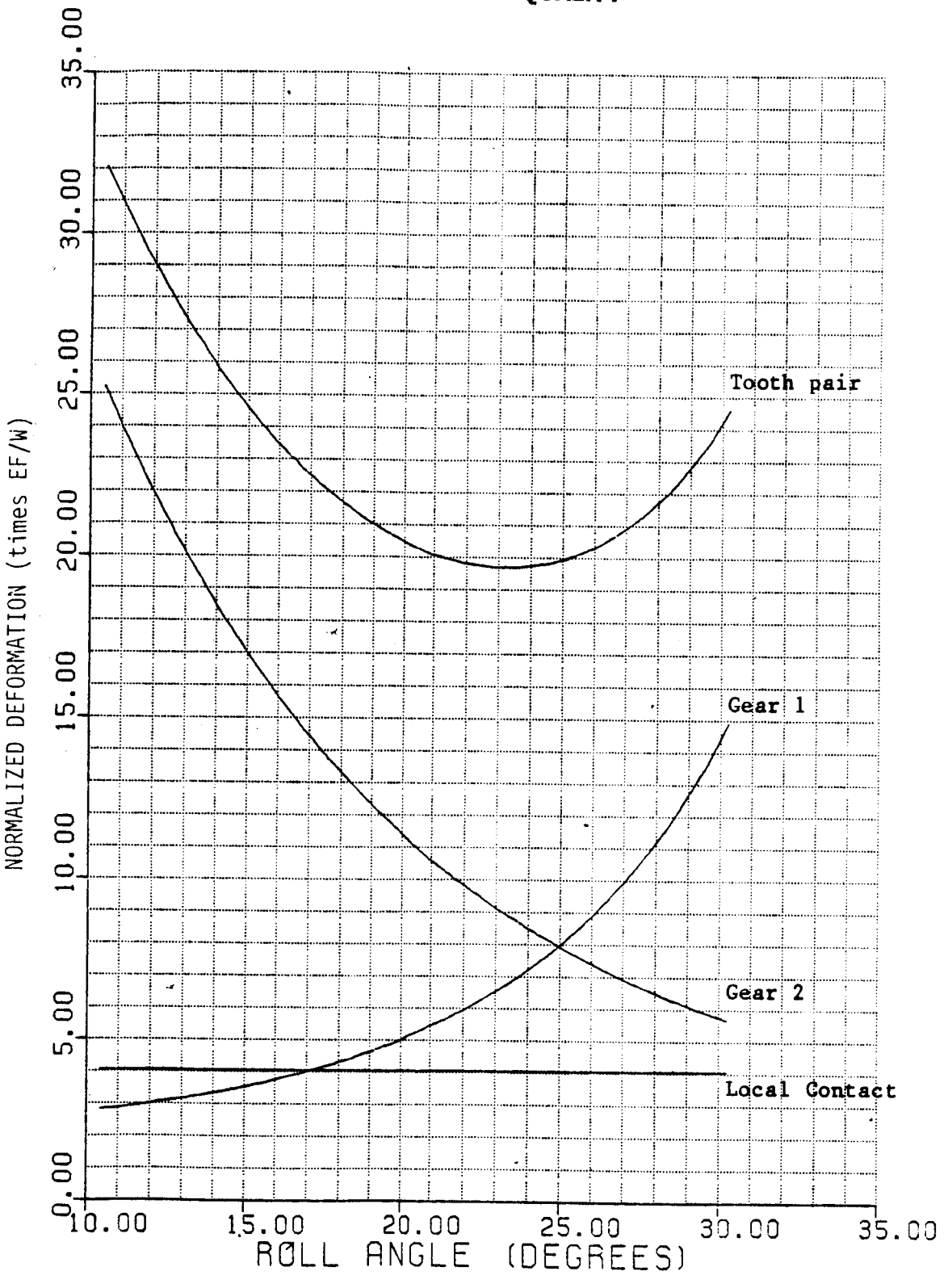

Figure II.11 Normalized Deformation of a Pair of Teeth, Diametral Pitch: 8; Pressure Angle: 20°; Pitch Radii: $R_{p1} = 2.25$, $R_{p2} = 6.75$ in.

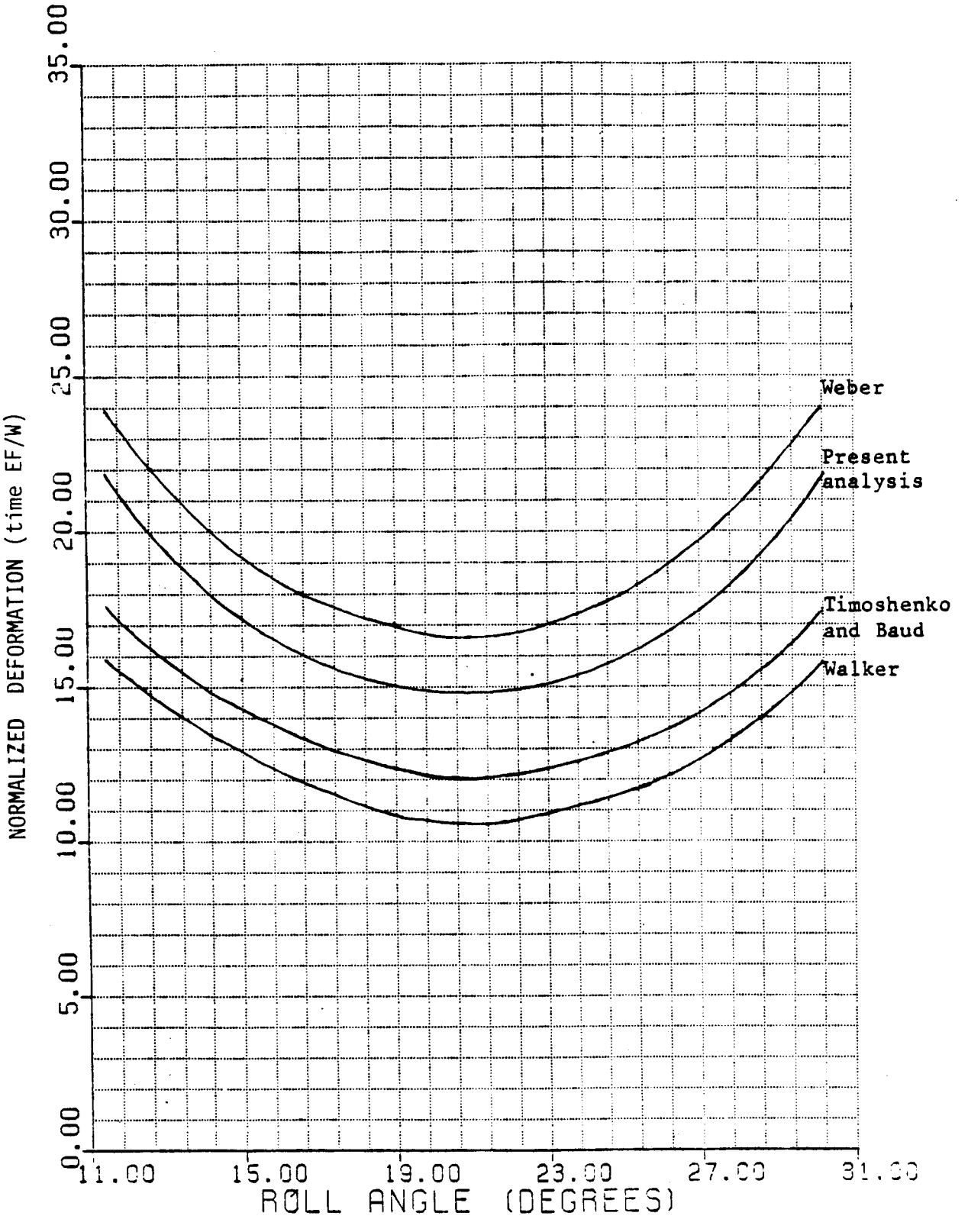

Figure II.12 Comparison of Results for Normalized Deformation of a Tooth pair, Diametral Pitch: 8; Pressure Angle: 20°; Pitch Radii: $R_{p1} = R_{p2} = 2.25$ in.

II.4 Mesh Analysis

II.4.1 Analysis of the Meshing Cycle

Figure II.13 illustrates the motion of a pair of meshing teeth. The initial contact occurs at A, where the addendum circle of the driven gear intersects the line of action. As the gears rotate the point of contact will move along the line of action, APD. When the tooth pair reaches B, the recessing tooth pair disengages at D leaving only one tooth pair in contact. From B through P to C is then a single contact zone for low contact ratio gears. When the tooth pair reaches point C, the next tooth pair begins engagement at A and starts another cycle.

In our analysis, the posiiton of the contact point of the gear teeth along the line of action is expressed in terms of roll angles of the driving gear tooth. This is therefore consistent with the analysis of gear tooth deflection and stiffness, which is also expressed in terms of roll angles of the driving gear tooth.

II.4.2 Transmission Error, Stiffness, and Load Sharing

Transmission error is defined as the departure of a meshing gear pair from the constant-angular speed ratio, as expected from the tooth number ratio. Transmission error is thus the measure of instantaneous variation from the ideal nominal value. Transmission error arises from the following sources:

1. Combined deflection of meshing teeth
2. Tooth spacing error
3. Tooth profile error
4. Runout error

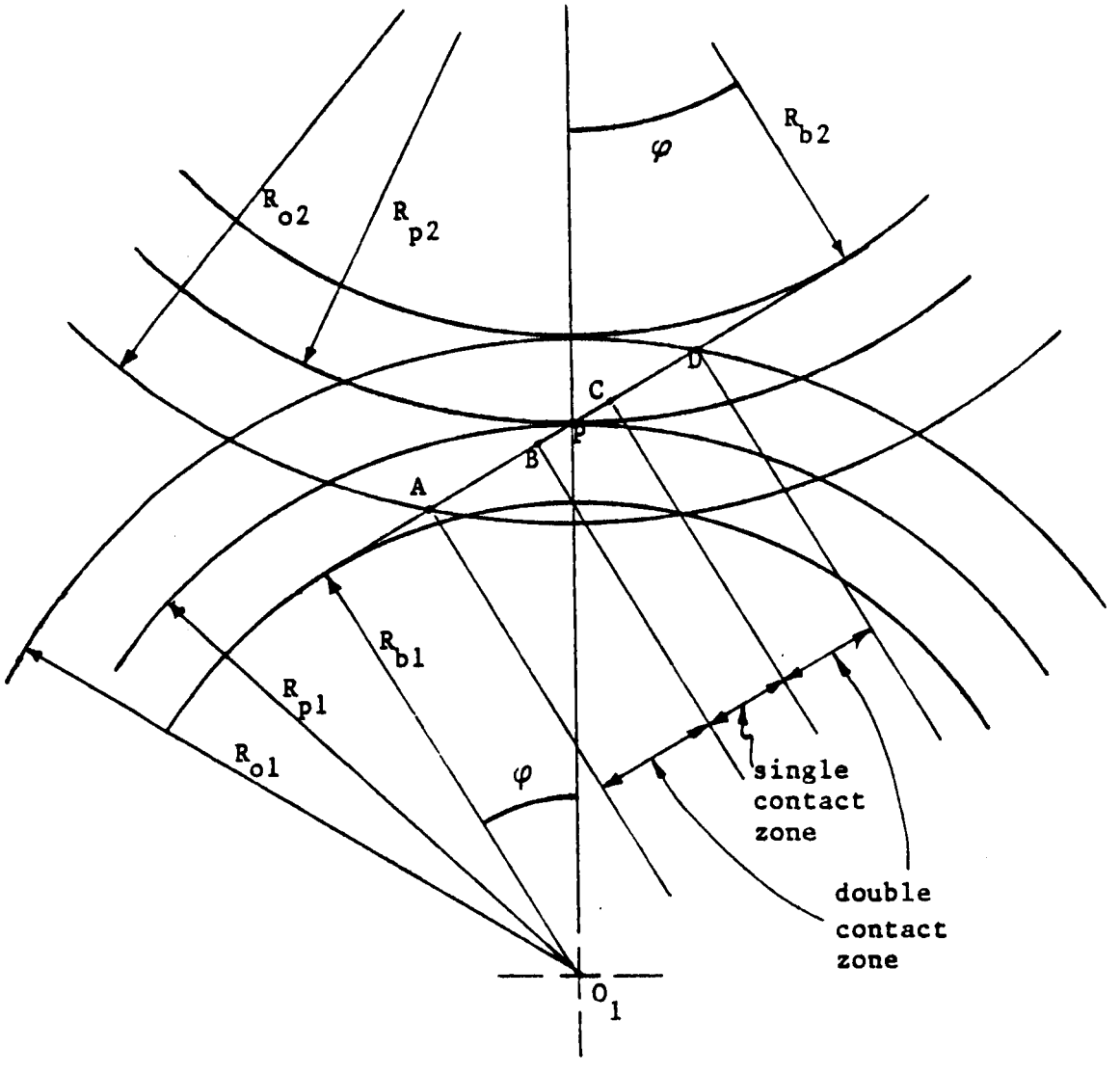

Figure II.13 Illustration of Gear Meshing Action

Usually the transmission error is expressed as an angular value. However, linear values are convenient for use in design and analysis computations. Specifically, in calculating the total transmission error for a meshed gear pair, the linear component values for each gear are often the same, whereas the angular values are a spectrum, inversely proportional to the pitch radii.

Transmission error and its components at the contact point may be expressed in the following notation: (The runout error is combined with the tooth spacing errors)

E_d: The deflection of gear teeth at the contact point.

E_s: The tooth spacing error. E_s is positive if the tooth spacing of the driven gear is less than the base pitch P_b, or if the tooth spacing of driving gear is greater than the base pitch P_b. Otherwise, E_s is negative.

E_p: The tooth profile error. E_p is positive if material is removed from the surface at the contact point. Alternatively, E_p is negative if material is added to the surface at the contact point.

E_t: The transmission error at the contact point. E_t is posistive if the driving gear leads the driven gear. Otherwise, E_t is negative.

Let the sequence of mating tooth pairs be designated by: a, b, c,...etc. Let the subscripts 1 and 2 designate the driving and driven gears respectively. Then the transmission error $(E_t)_j$ and the load sharing W_j at contact point j may be expressed as follows: For the double contact zone with tooth pairs a and b in contact, we have:

$$(E^a_t)_j = (E^a_{d1})_j+(E^a_{d2})_j+(E^a_{d2})_j+(E^a_{p1})_j+(E^a_{p2})_j \quad \text{(II.42)}$$

$$(E^b_t)_j = (E^b_{d1})_j+(E^b_{d1})_j+(E^b_{d2})_j+(E^b_{p1})_j+(E^b_{p2})_j+(E^b_{s1})_j+(E^b_{s2})_j \quad \text{(II.43)}$$

and

$$W^a_j + W^b_j = W \quad \text{(II.44)}$$

where W is the total transmitted load. For the single contact zone, with only tooth pair a in contact, we have:

$$(E^a_t)_j = (E^a_{d1})_j+(E^a_{d2})_j+(E^a_{p1})_j+(E^a_{p2})_j \quad \text{(II.45)}$$

and

$$W^a_j = W \quad \text{(II.46)}$$

To simplify the notation, we introduce the following items:

$$(E_s)_j = (E_{s1})_j + (E_{s2})_j \quad \text{(II.47)}$$

$$(E_p)_j = (E_{p1})_j + (E_{p2})_j \quad \text{(II.48)}$$

$$(E_d)_j = (E_{d1})_j + (E_{d2})_j = Q_j W_j \quad \text{(II.49)}$$

where Q_j is the compliance at contact point j. To simplify the analysis, we assume that the transmission error is the same for tooth pairs a and b when they are sharing the transmitted load. Hence, we have

$$(E^a{}_t)_j = (E^b{}_t)_j = (E_t)_j \quad \text{(II.50)}$$

Substituting from Equations (II.47), (II.48), (II.49) and (II.50) into Equations (II.42) and (II.43), we obtain the relation:

$$Q_j^a W_j^a + (E_p^a)_j = Q_j^b W_j^b + (E_p^b)_j + (E_s^b)_j \qquad \text{(II.50)}$$

Solving Equations (II.44) and (II.51) for W_j and W_j give the results:

$$W_j^a = [Q_j^b W + (E_p^b)_j + E(E_s^b)_j - (E_p^a)_j] \,/\, (Q_j^a + Q_j^b) \qquad \text{(II.51)}$$

$$W_j^b = [Q_j^a W + (E_p^a)_j - (E_p^b)_j v - (E_s^b)_j] \,/\, (Q_j^a + Q_j^b) \qquad \text{(II.52)}$$

If all errors except tooth deflection are ignored then W_j^a and W_j^b are:

$$W_j^a = (Q_j^b W) \,/\, (Q_j^a + Q_j^b)$$

$$W_j^b = (Q_j^a W) \,/\, (Q_j^a + Q_j^b) \qquad \text{(II.55)}$$

Figure II.14 shows typical stiffness and load sharing characteristics of a low contact ratio gear with tooth deflection but no other transmission errors. Let a series of mating tooth pairs be denoted as a, b, c, d and let points A, B, P, C, D be the same as those in Figure II.13. Then, AB and CD represent the double contact regions, BC represents the single contact region, and P is the pitch point.

The stiffness values at double contact regions are clearly much higher than those at single contact regions. When gears rotate at appreciable speed, this time-varying stiffness as shown in Figure II.16 is the major exictation source for the dynamic response of gear systems.

The total transmitted load is shared between two pairs of teeth within double contact regions. The magnitude of the load shared by each individual tooth pair depends on the stiffness of that tooth pair. The higher the stiffness, the higher the shared load.

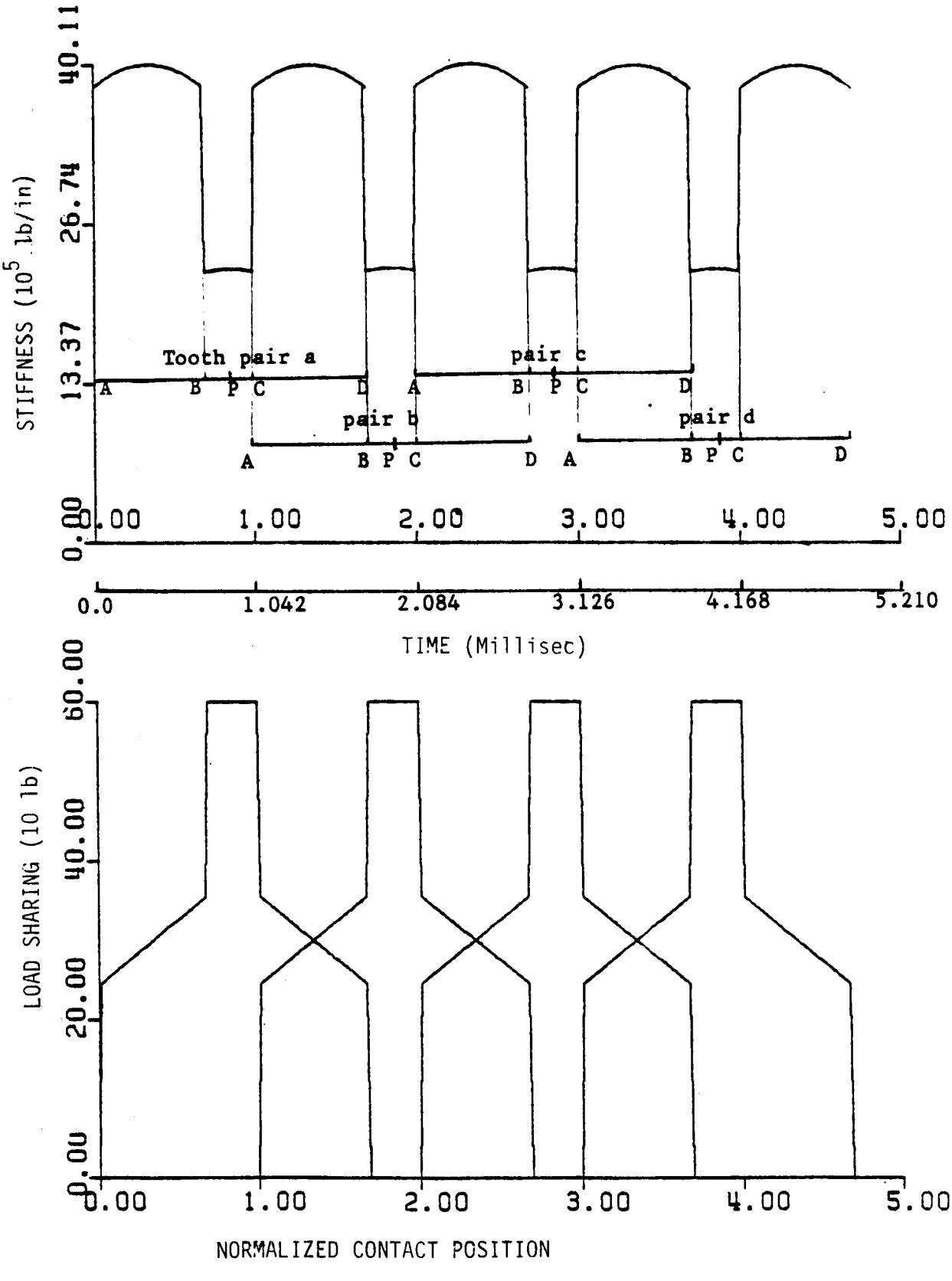

Figure II.14 Stiffness and Load Sharing of Low Contact Ratio Gears as in Figure II.10, at 1600 rpm.

II.5 Lubrication and Friction

II.5.1 Boundary, Mixed, and Hydrodynamic Lubrication

A purpose of lubrication is the reduction of friction between mating surfaces. The relative motion between mating gear teeth produces sliding and rolling friction which can be reduced but not totally eliminated. The friction developed depends upon the following:

(1) The characteristics of the lubricant.

(2) The pressure exerted between the contacting bodies.

(3) The nature and condition of the contacting surfaces.

(4) The ambient and surface temperatures.

There are four basic cases of lubrication which may be described as follows:

1. Boundary Lubrication: In this case the friction is mainly due to the interaction of asperities of the contacting surfaces.
2. Mixed Lubrication [Partial Elastohydrodynamic(EHD) Lubrication]: In this case the friction is created by both the interaction of asperities and by elastohydrodynamic effects.
3. Elastohydrodynamic (EHD) Lubrication: In this case there is no interaction of the asperities. The friction is a function of the fluid properties of the lubricant and in certain situations, the surface quality. The mating surfaces deform elastically.
4. Hydrodynamic Lubrication: This case is the same as EHD Lubrication except that there is no deformation of the mating surfaces.

Figure II.15 illustrates that these four cases, and Figure II.16 shows a representation of the friction coefficient for the four cases.

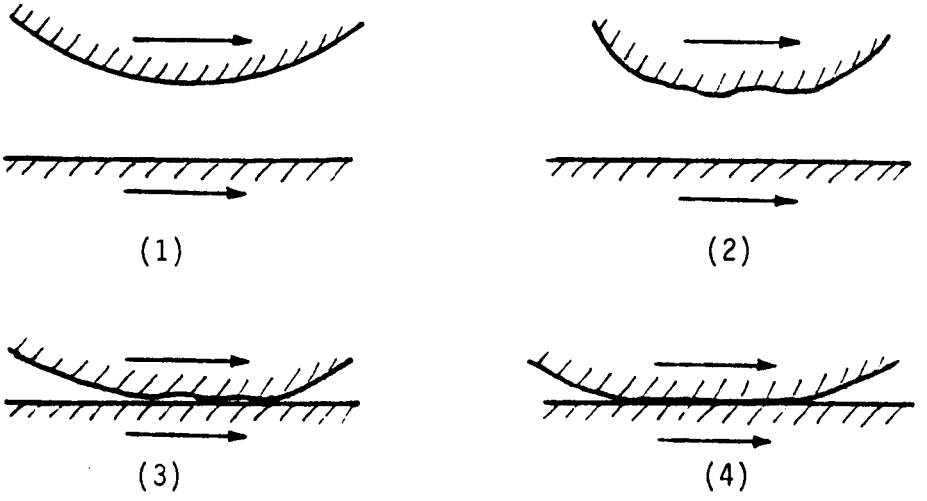

Figure II.15 Lubrication Cases: (1) Hydrodynamic; (2) Elastohydrodynamic (EHD); (3) Mixed; (4) Boundary.

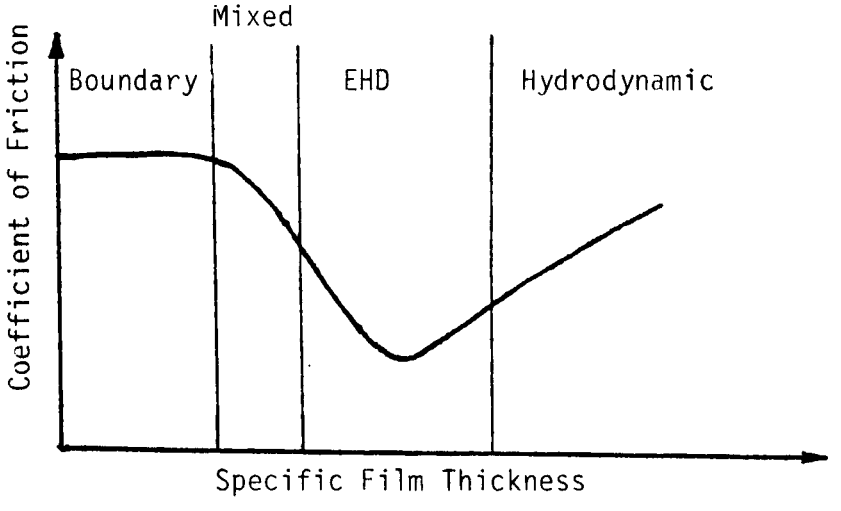

Figure II.16 Coefficient of Friction of Different Lubrication Cases

An important parameter for separating regimes is the specific film thickness λ, defined as:

$$\lambda = h_{min} / S" \qquad (II.56)$$

where h_{min} is the EHD minimum oil film thickness and S" is the composite surface roughness. S" may be expressed as:

$$S" = \sqrt{S_1^2 + S_2^2} \qquad (II.57)$$

The surface roughness varies for S_1 and S_2 are normally arithmetic-average (AA) values. [Formerly, root-mean-square (RMS) values were used for surface finish. The RMS value is approximatley 1.11 times the AA value.]

For Boundary Lubrication, λ is less than 1 ($\lambda<1$), and the gears may be thought of as running wet with oil. In this case the thickness of the oil film is quite small compared with the surface roughness. Essentially full surface-to-surface contact is obtained in the Hertzian contact band area. This is typical of slow-speed, high-load gears running with a rough surface finish. Hand-operated gears in winches, food presses, and jacking devices are typical of such gears.

For Mixed Lubrication λ is between 1 and 5 ($1<\lambda<5$), and partial surface-to-surface contact. The asperities of the tooth surfaces collide with each other, but substantial areas of the surfaces are separated by a thin film. Mixed Lubrication is typical of medium-speed gears with a good surface finish, which are heavily loaded, and which are running with relatively viscous oil. Most vehicle gears run under mixed lubrication.

For EHD Lubrication λ is between 1 and 10 ($1<\lambda<10$) and for Hydrodynamic Lubrication λ is greater than 10 ($\lambda>10$). In these cases, the oil film between contacting tooth surfaces is thick enough to avoid surface-to-surface contact. Even high asperities miss each other. Precision, high-speed gears generally operate under these lubrication conditions. Turbine-gears in ship drives, gears in electric generators, and gears in compressors are examples. In the aerospace industry, turboprop drives and helicopter main rotor gears operate in this region. An exception may be some final-stage gears which may run slowly enough to be in the mixed lubrication region.

References [17, 18, 19 and 31] provide additional details about the lubrication cases and about surface finishes.

II.5.2 Coefficient of Friction, Frictional Torques

There is a lack of agreement as to the proper form and variation of the friction coefficient. Buckingham [1] has recorded a semiempirical formula for the friction coefficient f as:

$$f = 0.05e^{-0.125V_s} + 0.002\sqrt{V_s} \qquad \text{(II.58)}$$

where V_s is the sliding speed measured in in/sec. An analogous expressions has been developed by Benedict and Kelly [22] and by Anderson and Lowenthal [23]:

$$f = 0.0127 \log (45.94\ W/F\mu_o\ V_s V_R^2) \qquad \text{(II.59)}$$

where W is the applied load, measured in lb, F is the face width, measured in inches, V_R is the rolling velocity, measured in in/sec, and

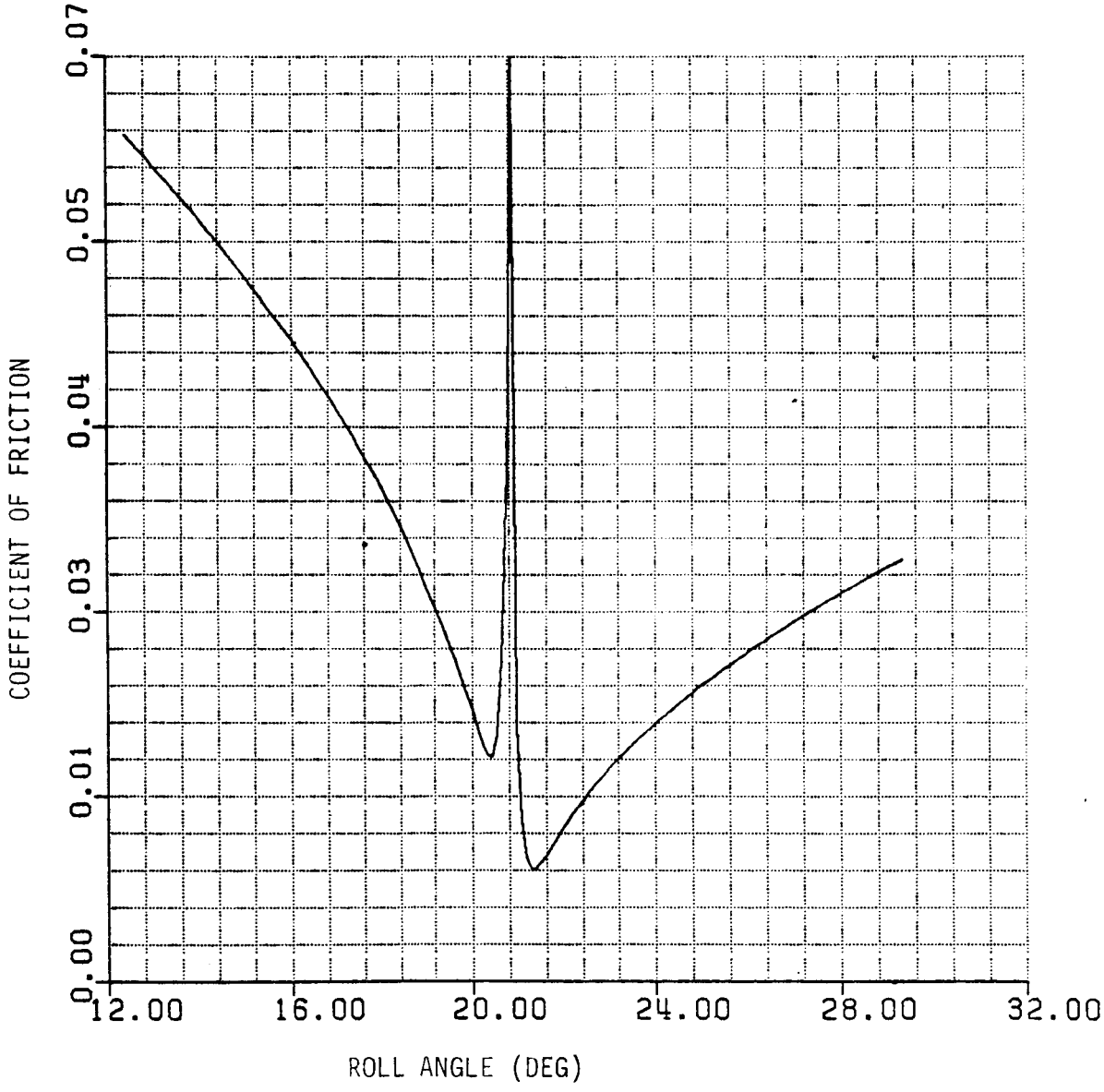

Figure II.17 Friction Coefficient Using Buckingham's Model

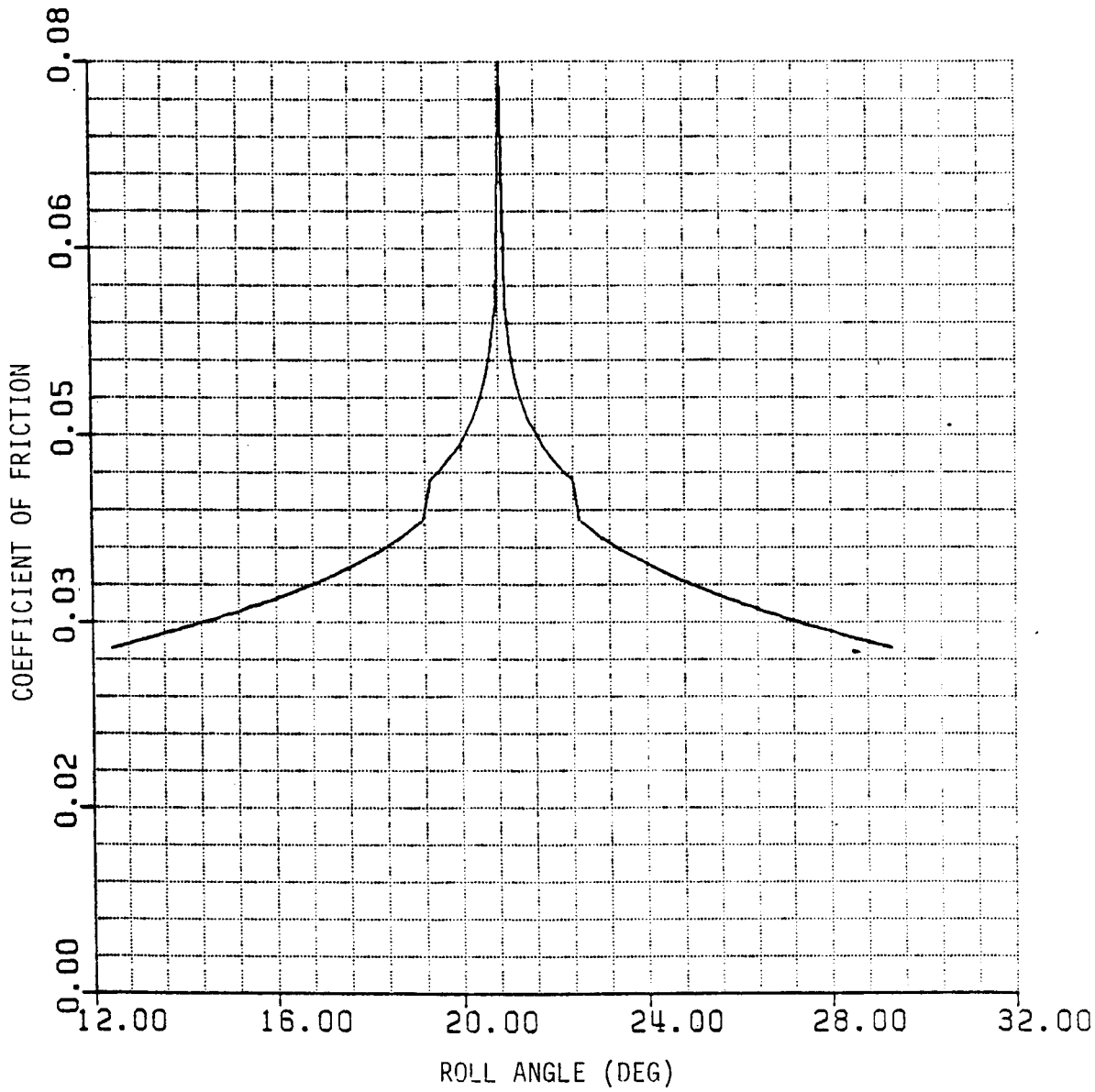

Figure II.18 Friction Coefficient Using Benedict and Kelley's Model

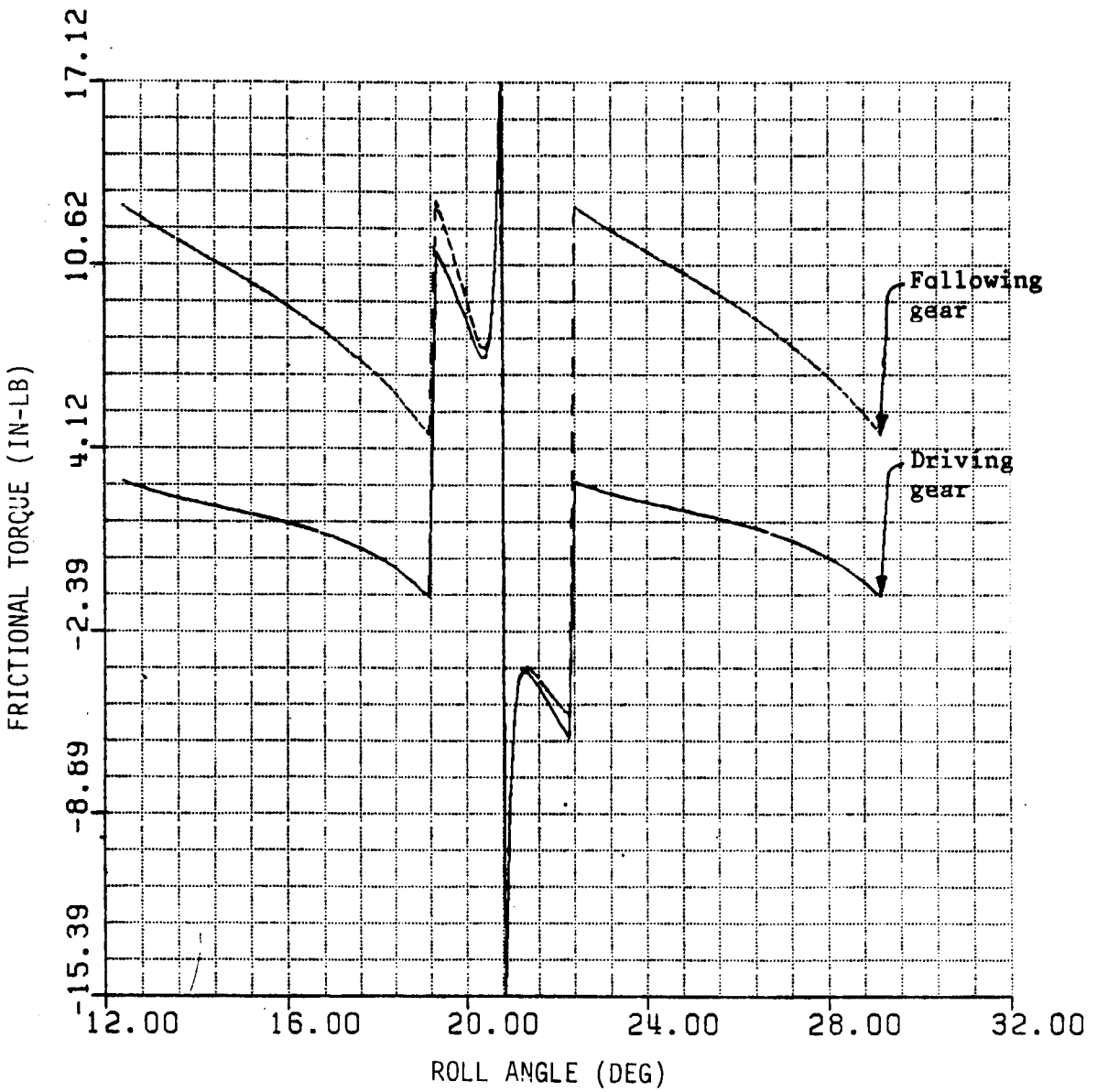

Figure II.19 Friction Torques Variation Along the Contact Path Using Buckingham's Model

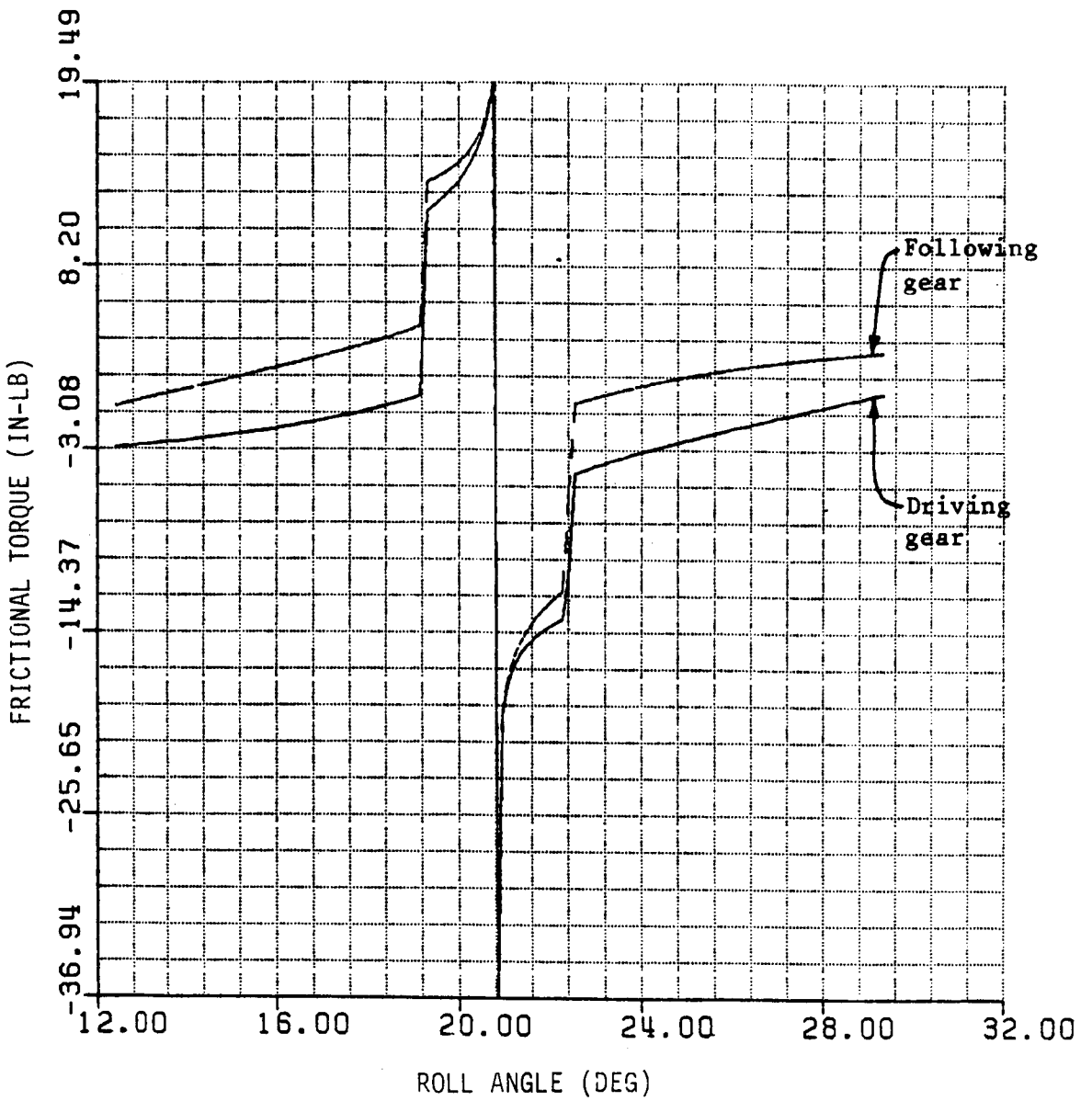

Figure II.20 Friction Torque Variation Along the Contact Path Using Benedict and Kelley's Model

μ_o is the lubricant viscoscity, measured in lb sec/in.

Figures II.17 and II.18 show graphs of the friction coefficient as given by Equations (II.58) and (II.59) as a function of the roll angle. Figures II.19 and II.20 show the resulting effect upon the friction torque.

Finally, it should be noted that Equation (II.59) is valid only when the specific film thickness λ [See Equation (II.56)] has values between 1 and 2. However, this is the range of many gear applications of interest. Moreover, extending the use of Equation (II.59) to systems with higher values of λ should not introduce serious errors.

II.6 Shafts and Connected Masses

The shafts and connected masses are also components of the gear system. The parameters related to dynamic system response are the polar mass moment of inertia, and the stiffness of shafts and masses.

For bodies with annular cross-section, outside diameter D_o, inside diameter D_i, the polar area moment of inertia J is:

$$J = \frac{\pi}{32} (D_o^4 - D_i^4) \qquad \text{(II.60)}$$

The torsional shaft stiffness K is then given by:

$$K = JG/\ell \qquad \text{(II.61)}$$

where G is the shear modulus and ℓ is the shaft length.

The polar mass moment of inertia I is given by the expression:

$$I = \frac{1}{8} m(D_o^2 - D_i^2) \qquad \text{(II.62)}$$

where m is the shaft mass.

III. SYSTEM DYNAMIC ANALYSIS

III.1 Dynamic Analysis and Computational Procedure

III.1.1 Mathematical Modelling and Equations of Motion

The system model as shown in Figure II.2 is used for the dynamic analysis. Its mathematical model, shown in Figure II.1, and the resulting governing equations are developed using basic gear geometry and elementary vibration principles. The equations may be expressed as follows:

$$J_M\ddot{\theta}_M + C_{s1}(\dot{\theta}_M - \dot{\theta}_1) + K_{s1}(\theta_M - \theta_1) = T_M$$

$$J_1\ddot{\theta}_1 + C_{s1}(\dot{\theta}_1 - \dot{\theta}_M) + K_{s1}(\theta_1 - \theta_M) + C_g(t)[R_{b1}\dot{\theta}_1 - R_{b2}\dot{\theta}_2]$$
$$+ K_g(t)\,[R_{b1}(R_{b1}\theta_1 - R_{b2}\theta_2)] = T_{f1}(t)$$

$$J_2\ddot{\theta}_2 + C_{s2}(\dot{\theta}_2 - \dot{\theta}_1) + K_{s2}(\theta_2 - \theta_1) + C_g(t)[R_{b2}\dot{\theta}_2 - R_{b1}\dot{\theta}_1]$$
$$+ K_g(t)\,[R_{b2}(R_{b2}\theta_2 - R_{b1}\theta_1)] = T_{f2}(t)$$

$$J_L\ddot{\theta}_L + C_{s2}(\dot{\theta}_L - \dot{\theta}_2) + K_{s2}(\theta_L - \theta_2) = -T_L \qquad \text{(III.1)}$$

where the notation is

θ, $\dot{\theta}$, $\ddot{\theta}$ — angular displacement, velocity and acceleration

θ_M, θ_1, θ_2, θ_L — angular displacement of motor, gears 1 and 2, and the load

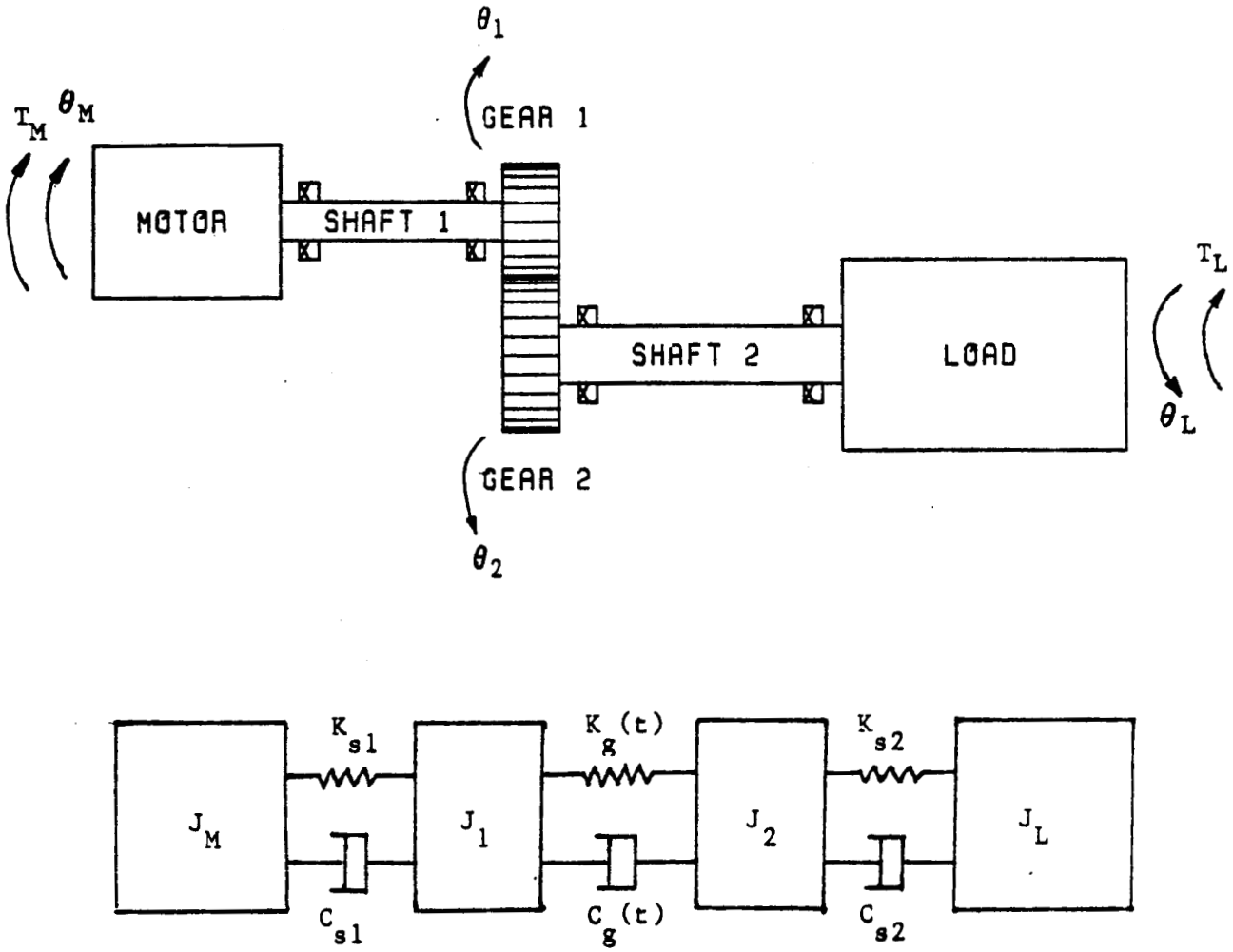

Figure III.1 A Spur Gear System and Its Mathematical Model.

J_M, J_1, J_2, J_L mass moments of inertia of the motor, gears 1 and 2 and the load.

C_{s1}, C_{s2}, $C_g(t)$ damping coefficients of the shafts and gear teeth.

T_M, T_L, $T_{f1}(t)$, $T_{f2}(t)$ input and output torques and frictional torques on the driving (1) and driving (2) gears.

The procedures developed in Part II are used to determine the spring stiffness, modelling the elastic behavior of the gear teeth. The equations of motion will thus be dependent upon excitation terms due to transmission errors. However, it is a difficult task even under ideal geometry conditions to obtain a precise modelling of the dynamic loading. The vibration of the gear tooth is affected by irregularity in motion due to manufacturing errors and by deflections of the tooth due to the applied loads. The motion is further affected by other teeth leaving contact. The motion becomes more complicated when the teeth begin to assume the entire load, resulting in a complex vibratory motion taking place in the zone of single contact.

The meshing process leads to instantaneous load fluctuations in the teeth even under constant loading conditions. Also, the magnitude of the load and the fluctuations are influenced by the damping effect of the lubricant, and the proximity to system natural frequencies of the operating frequencies.

Several assumptions are needed to simplify the analysis:

1. The dynamic process is defined in the rotating plane of the gears. The out-of-plane twisting and misalignment are neglected.

2. Damping due to lubrication of the gears and shafts are expressed as constant damping coefficients.
3. The differential equations of motion are developed using the theoretical line of action.
4. Gear tooth stiffness is evaluated according to dynamic considerations: That is, the reference point for tooth deflection is assumed to be located at the radius of gyration.
5. Low contact ratio gear pairs are used in the analysis. The contact ratio is taken between 1 to 2.

III.1.2 Computational Procedure

Equations (III.1) are solved using a linearized-iterative procedure. The linearized equations are obtained by dividing the mesh period into n equal intervals. In the analysis a constant input torque T_M is assumed. However, the output torque T_L is assumed to be fluctuating due to damping in the gear mesh, friction, and time-varying mesh stiffness. Finally, a true involute profile is assumed.

Initial values of the angular displacements are obtained by preloading the input shaft with the nominal torque carried by the system. Initial values of the angular speeds are taken from the nominal operating speed of the system.

The iterative process is as follows: The calculated values of the angular displacements and angular speeds after one period, are compared with the assumed initial values. Unless the differences between them are sufficiently small, the procedure is repeated using the average of the initial and calculated values as new initial values. The criteria for repeating is:

$$|\theta_n - \theta_o| > 0.001\ \theta_o$$

and

$$|\dot{\theta}_n - \dot{\theta}_o| > 0.001\ \dot{\theta}_o \qquad \text{(III.2)}$$

The term $(R_{b1}\ \theta_1 - R_{b2}\ \theta_2)$ in the equations of motion represents the relative dynamic displacement of the gears. Let Bh represent the backlash. Let gear 1 be the driving gear. The following conditions can occur:

Case (i)

$$R_{b1}\ \theta_1 - R_{b2}\ \theta_2 > 0 \qquad \text{(III.3)}$$

This is the normal operating case and the dynamic mesh force W_d is defined as:

$$W_{d1} = K_g(t)(R_{b1}\ \theta_1 - R_{b2}\theta_2) + C_g(t)(R_{b1}\dot{\theta}_1 - R_{b2}\dot{\theta}_2) \qquad \text{(III.4)}$$

and

$$W_{d2} = W_{d1} \qquad \text{(III.5)}$$

Case (ii)

$$R_{b1}\theta_1 - R_{b2}\theta_2 \leq 0 \quad \text{and} \quad |R_{b1}\theta_1 - R_{b2}\theta_2| \leq Bh \qquad \text{(III.6)}$$

In this case, the gears will separate and the contact between the gears will be lost. Hence,

$$W_d = 0 \qquad \text{(III.7)}$$

Case (iii)

$$R_{b1}\theta_1 - R_{b2}\theta_2 < 0 \quad \text{and} \quad |R_{b1}\theta_1 - R_{b2}\theta_2| > Bh \qquad \text{(III.8)}$$

In this case, gear 2 will collide with gear 1 on the backside. Then,

$$W_{d1} = K_g(t)[(R_{b2}\theta_2 - R_{b1}\theta_1) - Bh] + C_g(t)(R_{b1}\dot{\theta}_1 - R_{b2}\dot{\theta}_2) \tag{III.9}$$

and

$$W_{d2} = W_{d1} \tag{III.10}$$

The equations of motion contain damping terms for all components in the system. The damping in the shafts is due to material damping. Experiments have suggested that this damping is between 0.5% and 0.75 of the critical damping (See Reference [35].) Hence, the effective damping of shafts is taken as

$$C_{s1} = 2\xi_s \sqrt{K_{s1}/(1/J_D + 1/J_1)} \tag{III.11}$$

and

$$C_{s2} = 2\xi_s \sqrt{K_{s2}/(1/J_L + 1/J_2)} \tag{III.12}$$

where ξ_s represents the critical damping ratio of shafts with value: 0.005.

Similarly, the effective damping of the gear mesh is taken as:

$$C_g = 2\xi\left[\frac{k_g R_{b1}^2 R_{b2}^2 J_1 J_2}{R_{b1}^2 J_1 + R_{b2}^2 J_2}\right]^{\frac{1}{2}} \tag{III.13}$$

where ξ represents the critical damping ratio. Measurements of geared systems show ξ to range between 0.03 and 0.17 (See References [10, 11]). In Equation (III.13) the average gear mesh stiffness is used and the equivalent masses of the gears are concentrated at the base circle to reflect their effects along the line of action.

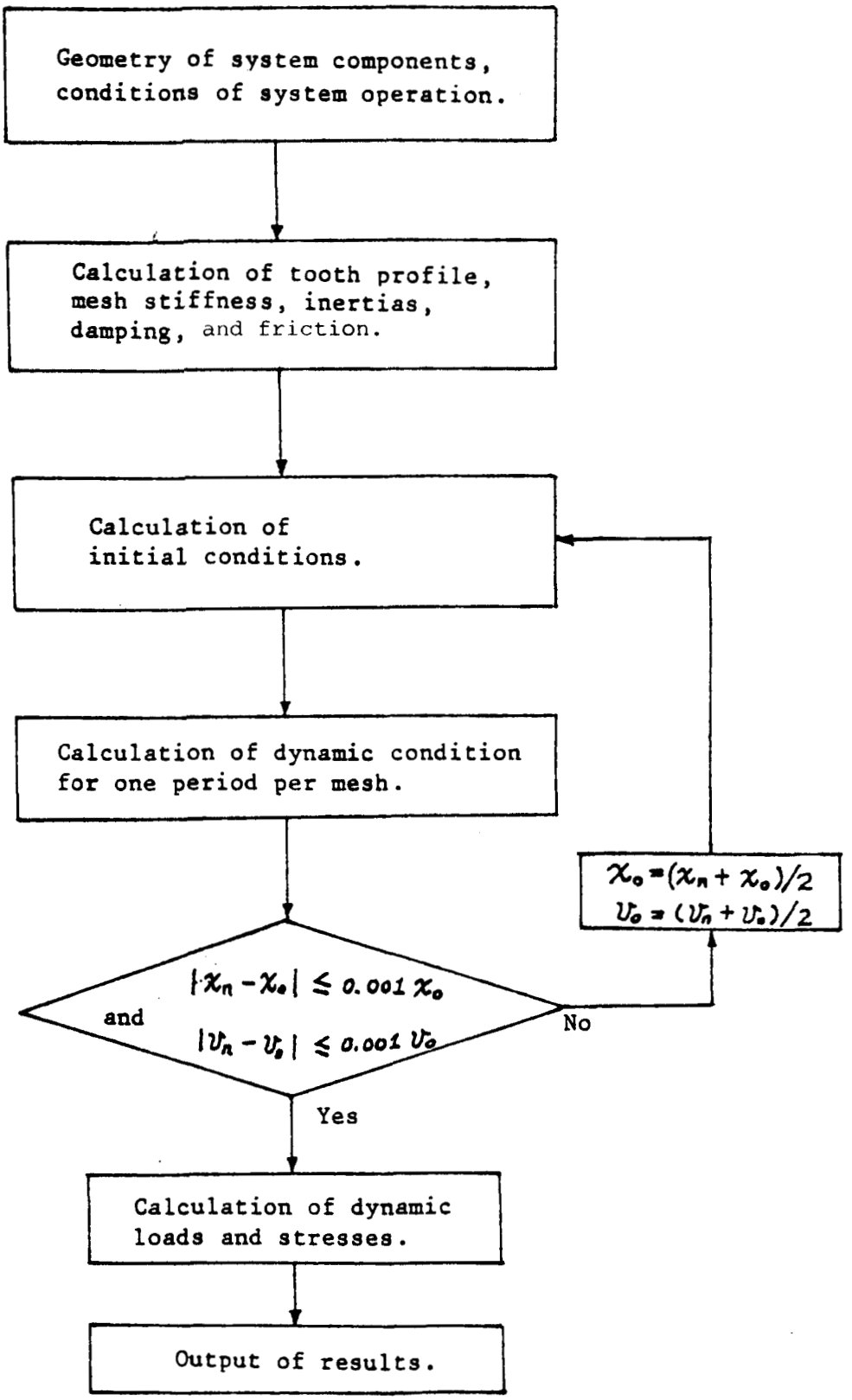

Figure III.2 Flow Chart of Computational Procedure

The flow chart of the computational procedure is shown in Figure III.2.

III.2 Natural Frequencies

The natural frequencies of the system may be obtained by examining the undamped equation of motion written in matrix form:

$$[J][\ddot{\theta}] + [K][\theta] = [0] \tag{III.14}$$

where the inertia matrix [J] is

$$[J] = \begin{bmatrix} J_D & 0 & 0 & 0 \\ 0 & J_1 & 0 & 0 \\ 0 & 0 & J_2 & 0 \\ 0 & 0 & 0 & J_L \end{bmatrix} \tag{III.15}$$

and the stiffness matrix [K] is

$$[K] = \begin{bmatrix} K_{s1} & -K_{s1} & 0 & 0 \\ -K_{s1} & K_{s1} + (K_g)_{avg} R_{b1} & -(K_g)_{avg} R_{b1} R_{b2} & 0 \\ 0 & -(K_g)_{avg} R_{b1} R_{b2} & K_{s2} + (K_g)_{avg} R_{b2} & -K_{s2} \\ 0 & 0 & -K_{s2} & K_{s2} \end{bmatrix}$$

The average value of gear mesh stiffness is taken as the sum of the discrete tooth stiffness values over one mesh cycle divided by the number of mesh positions in the cycle.

Equations (III.14) may thus be used to determine the eigenvalues and thus the natural frequencies of the system.

III.3 Parametric Study

A brief parametric study was conducted to determine the effects of the rotating speed, the load, the stiffnesses, the inertias, and the contact ratio on the dynamic load. The system examined consisted of two identical gears having the following properties:

Number of teeth: 36

Diametral pitch: 8

Pitch diameter: 4.5 in

Pressure angle: 20°

Face Width: 1.0 in

Moment of inertia: 0.02947 in lb sec^2

Stiffness: 3.5355×10^6 lb/in rad

Damping ratio: 0.10

The shaft stiffness, inertias were:

Shaft stiffness: 10081 in lb/rad

Motor and load inertia: 0.08841 in lb sec^2 (each)

Finally, the first three system critical speeds were:

ω : 89.6 rpm, 179.1 rpm, and 8688 rpm

For gears with true involute profile under normal operating conditions, the principal source of dynamic excitation is the time varying tooth stiffness due to alternating single and double contact of the tooth pairs. The gear system vibration depends upon the frequency of this parametric excitation, and thus also the operating speed.

III.3.1 Dynamic Load as a Function of Roll Angle

Figure III.3 shows the variation of dynamic load response for a pair of teeth as a function of roll angle. At lower speeds where the excitation frequency is much lower than the resonance frequency, the dynamic load response is basically a static load sharing in phase with the stiffness change, superimposed with an oscillatory load at a frequency corresponding to the natural frequency.

At higher speeds, close to the natural frequency, the dynamic load variation becomes so abrupt that it produces tooth separation. The peak dynamic load is much higher than the static load and is very likely a source of gear noise and early surface fatigue.

Figure III.4 shows the dynamic load response as a function of operating speed. The major peak occurs at the natural frequency. The second major peak occurs at the principal parametric resonance frequency due to the parametric excitation of the time varying tooth stiffness. This parametric resonance frequency is about half the system natural frequency [27]. Finally, the dynamic factor is defined as the ratio of dynamic load to static load.

Observe that for speeds above the natural frequency, the dynamic response decreases steadily in the same manner as with elementary vibratory systems.

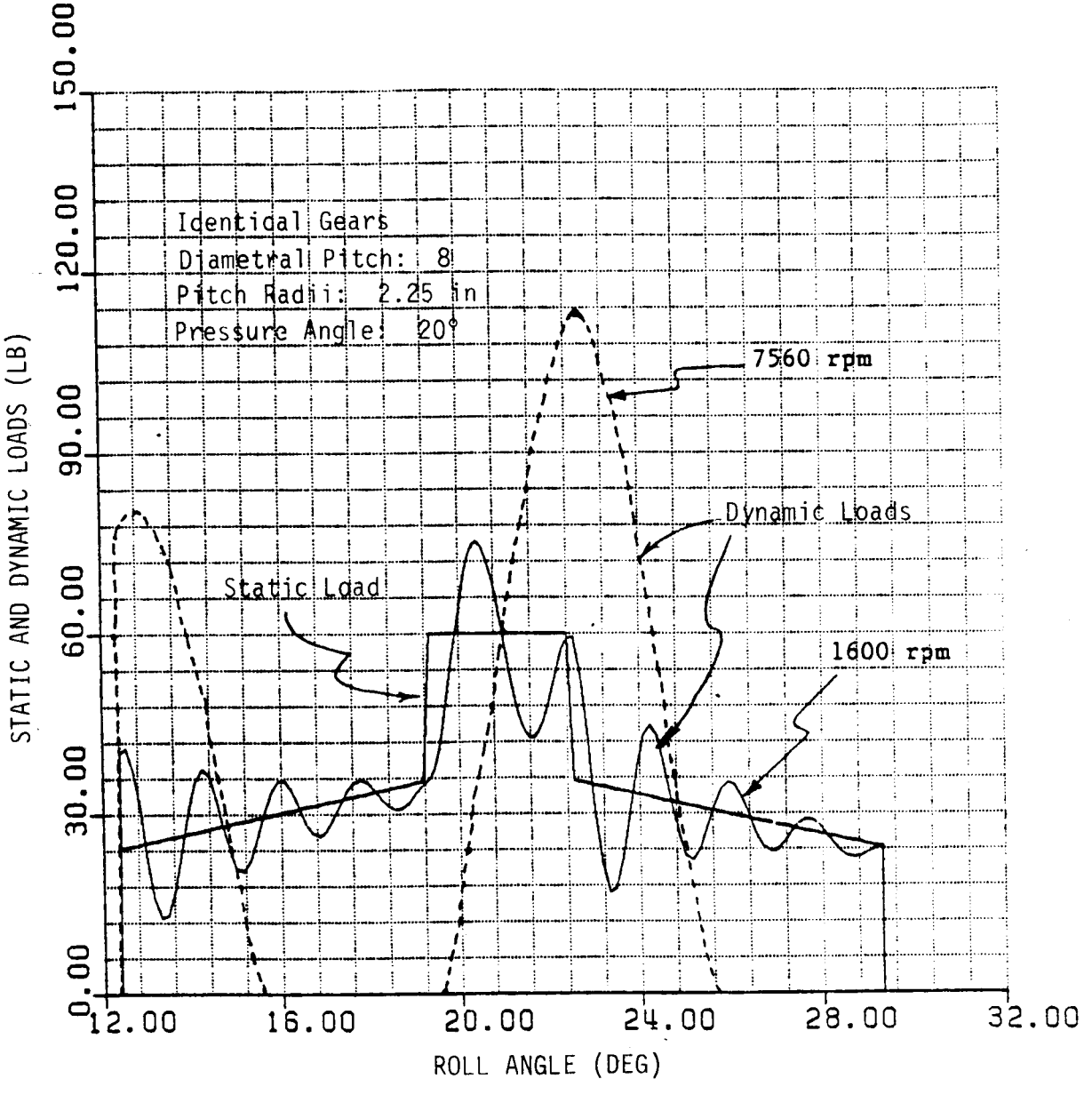

Figure III.3 Dynamic Loads at Different Speeds

Figure III.5 shows a three dimensional representation of the system dynamic response. The horizontal axis represents the operating speed, and the contact position along the tooth profile. The total number of contact positions is 121. The vertical axis is the dynamic factor, defined by the ratio of the dynamic load to the static load.

Figure III.6 presents a contour plot of the system dynamic response.

The shaded areas, represent regions where tooth separation occurs. They are located in the double contact regions. At near resonance speeds the vibration motion of gear bodies exceeds the deflection of the meshing tooth pairs, inducing tooth separation.

As the speed increases, the dynamic response also shows a phase shift towards the higher numbered contact positions. This phenonemon can be seen by noting that the highest dynamic effect (at speeds ranging from 600 rpm to 10400 rpm) occurs at different contact positions beginning from position 51 and gradually changing to position 85. This is an important factor when computing the root stresses.

III.3.2 Effect of the Applied Load

Figure III.7 shows the maximum dynamic load on the system as a function of the transmitted loads for different speeds.

The deflection of gear teeth changes the tooth stiffness and load sharing between the teeth. The separation of gear teeth due to vibration is resisted by the transmitted load. Therefore, the dynamic load effect is decreased as the applied load is increased.

III.3.3 Effect of Damping

The damping due to viscous friction governs the dynamic load response of the gear system. Figure III.8 shows the effect of damping on the dynamic load response. It is seen that the damping has a greater

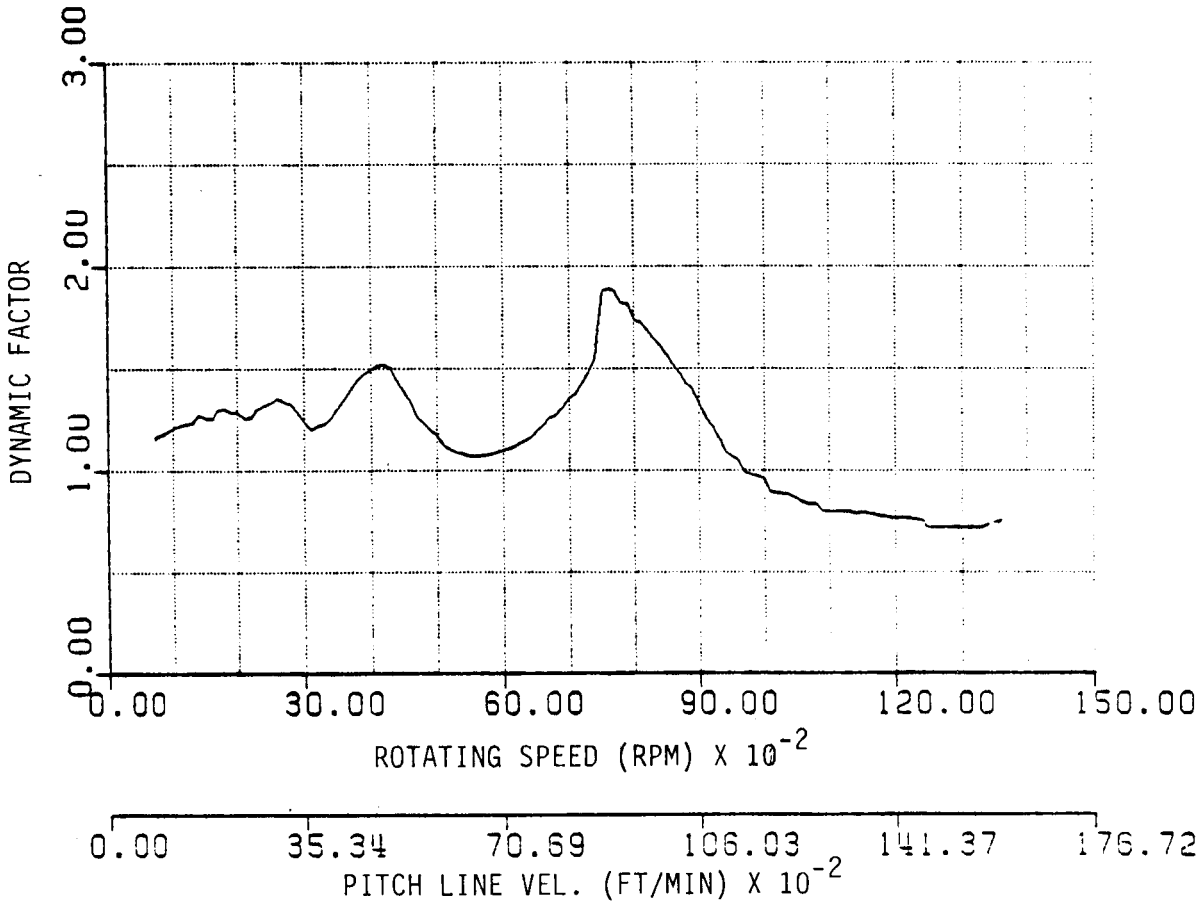

Figure III.4 Dynamic Load Response as a Function of Rotating Speed

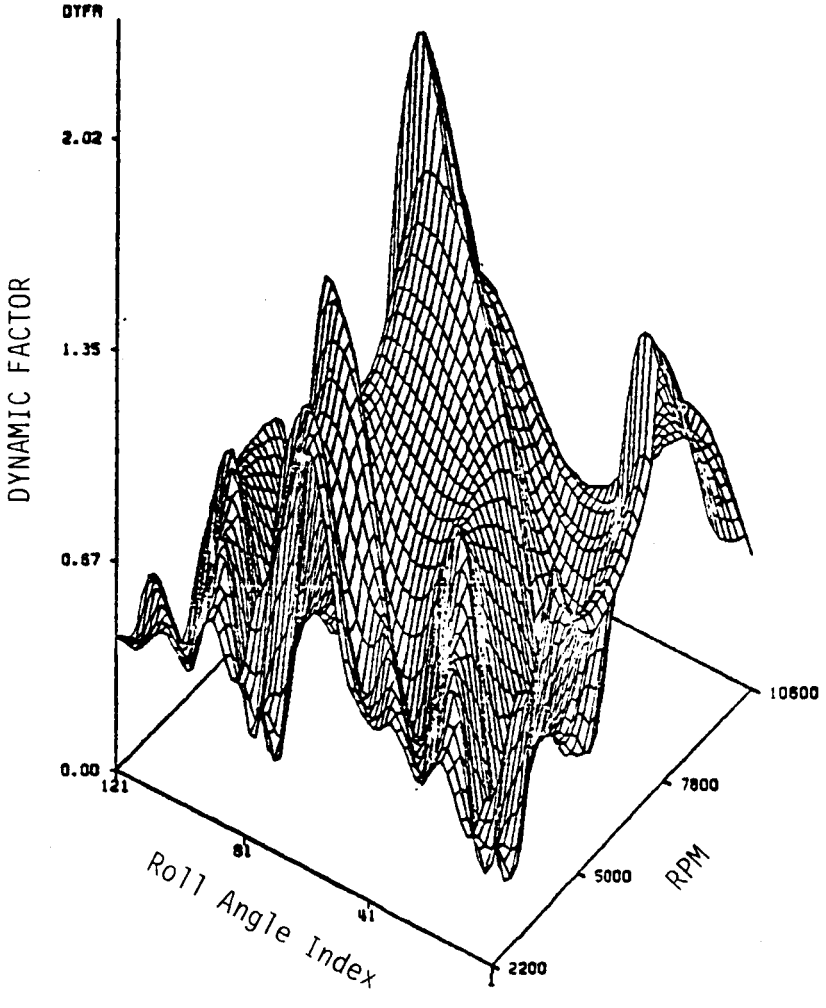

Figure III.5 System Dynamic Response

DYNAMIC RESPONSE OF SYSTEM

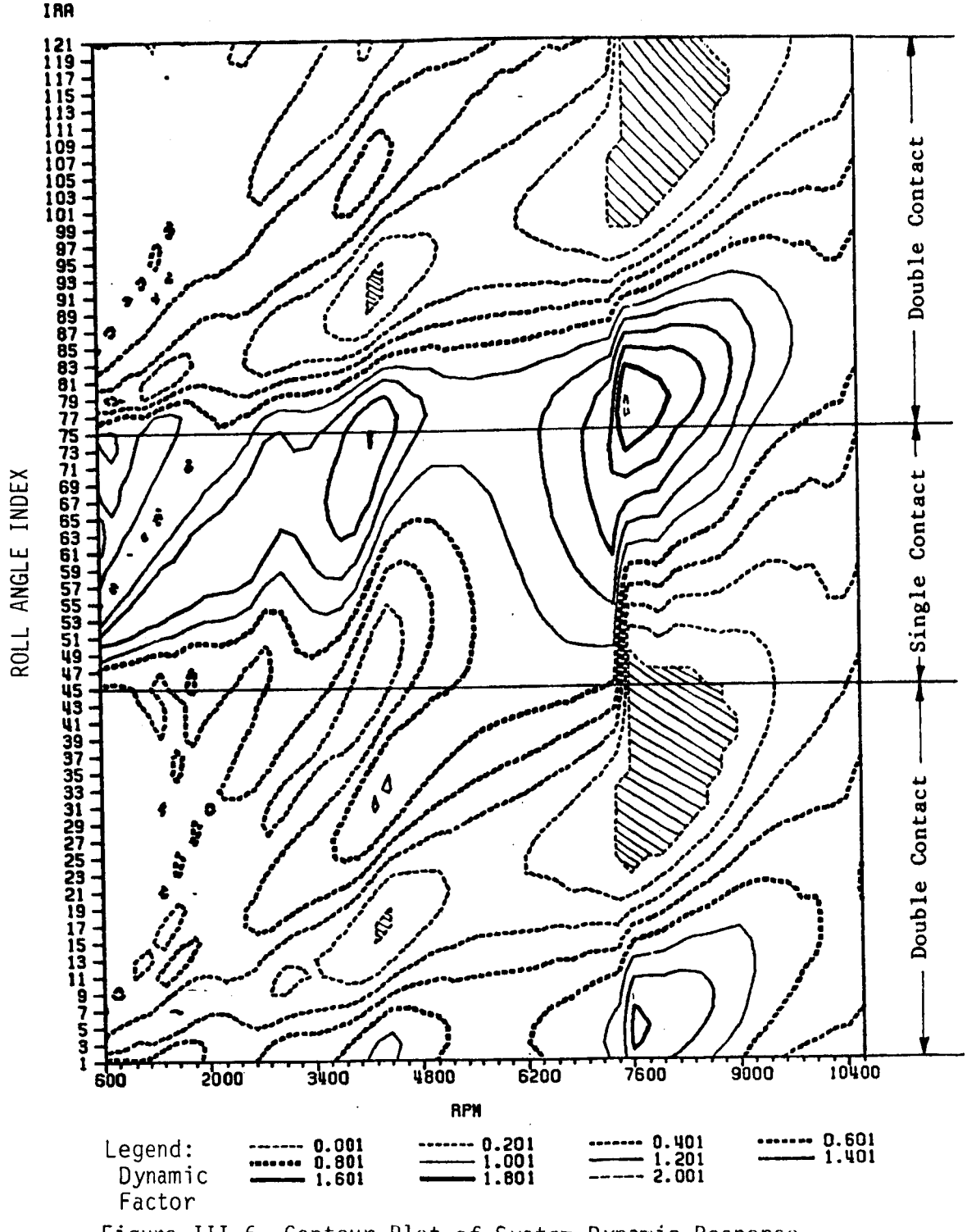

Figure III.6 Contour Plot of System Dynamic Response

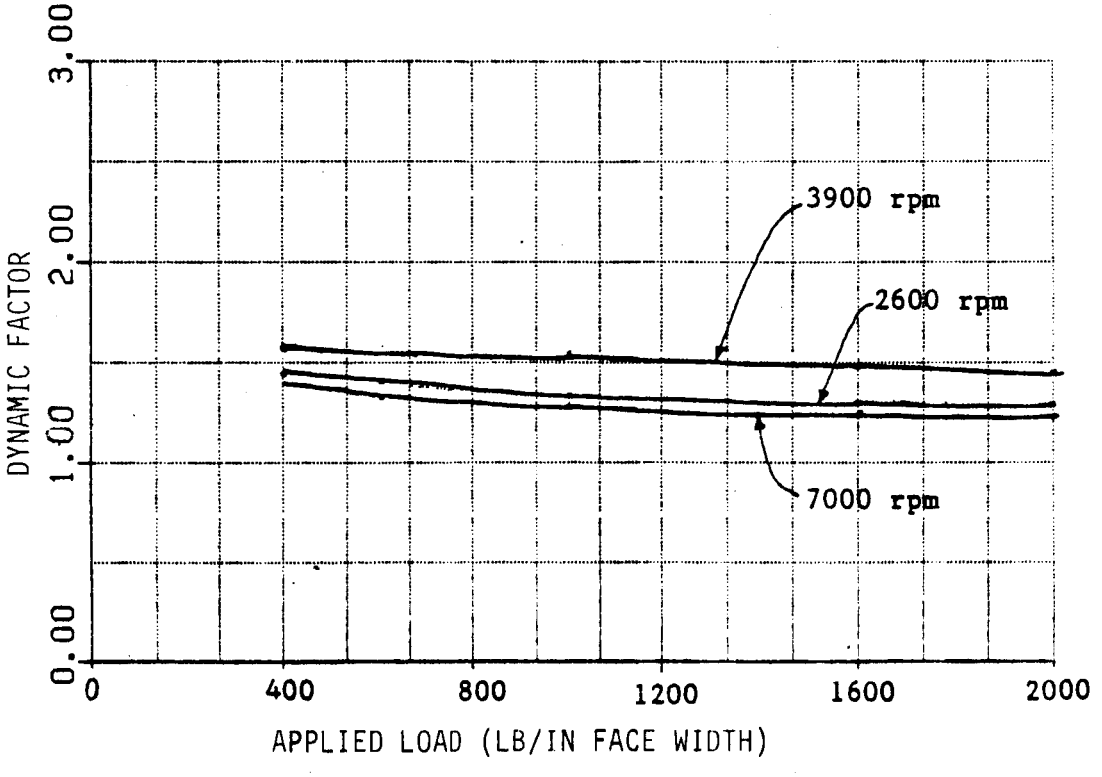

Figure III.7 Effect of Applied Load on the Dynamic Load Response

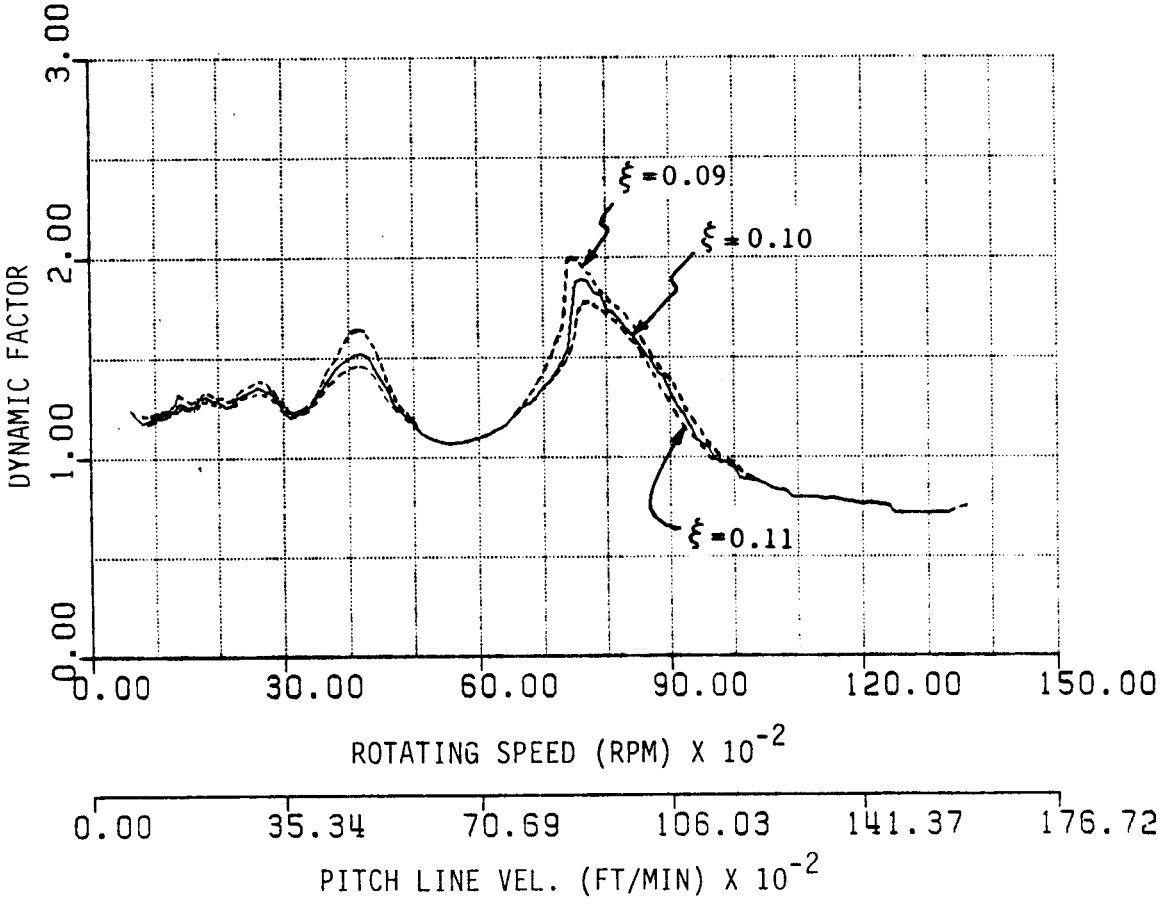

Figure III.8 Effect of Damping on the Dynamic Load Response

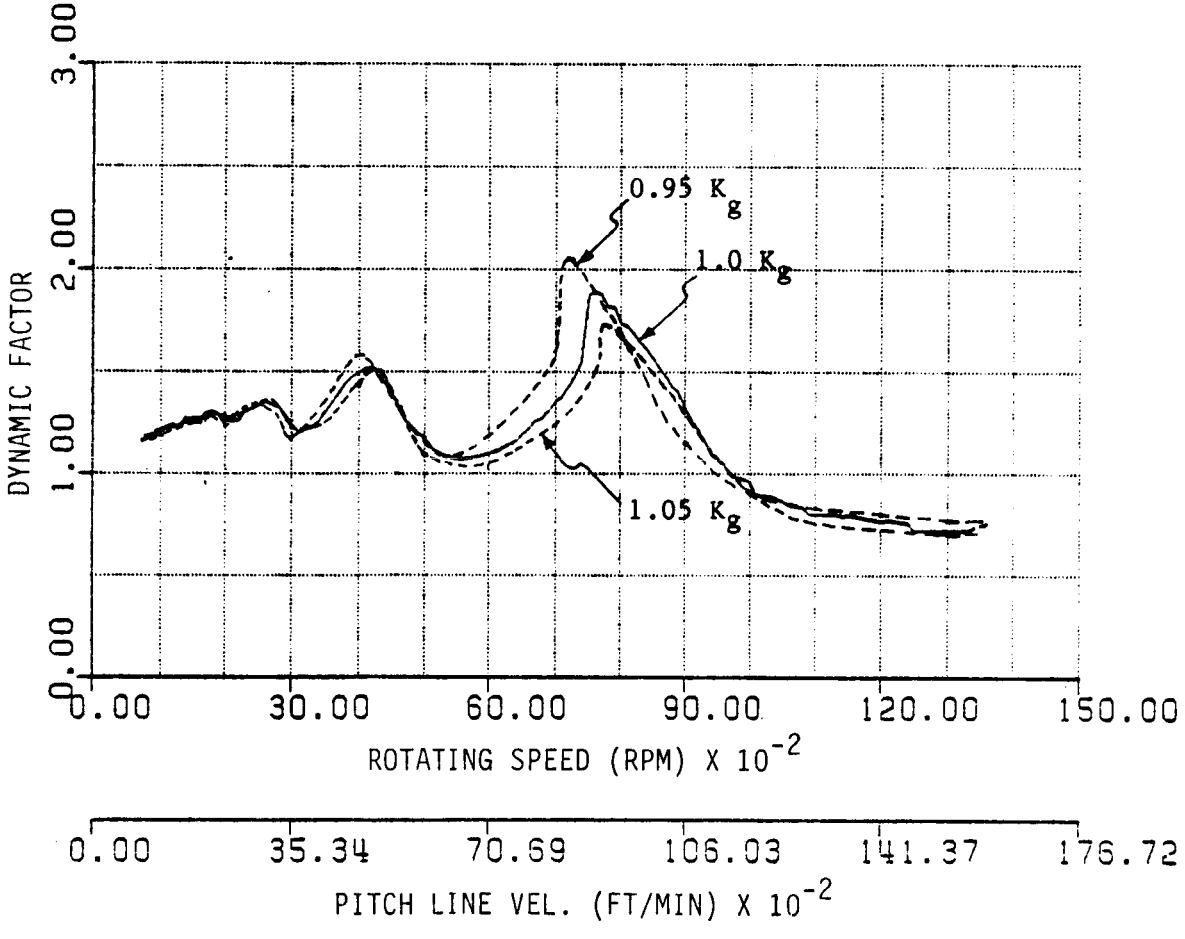

Figure III.9 Effect of Tooth Stiffness on Dynamic Load Response

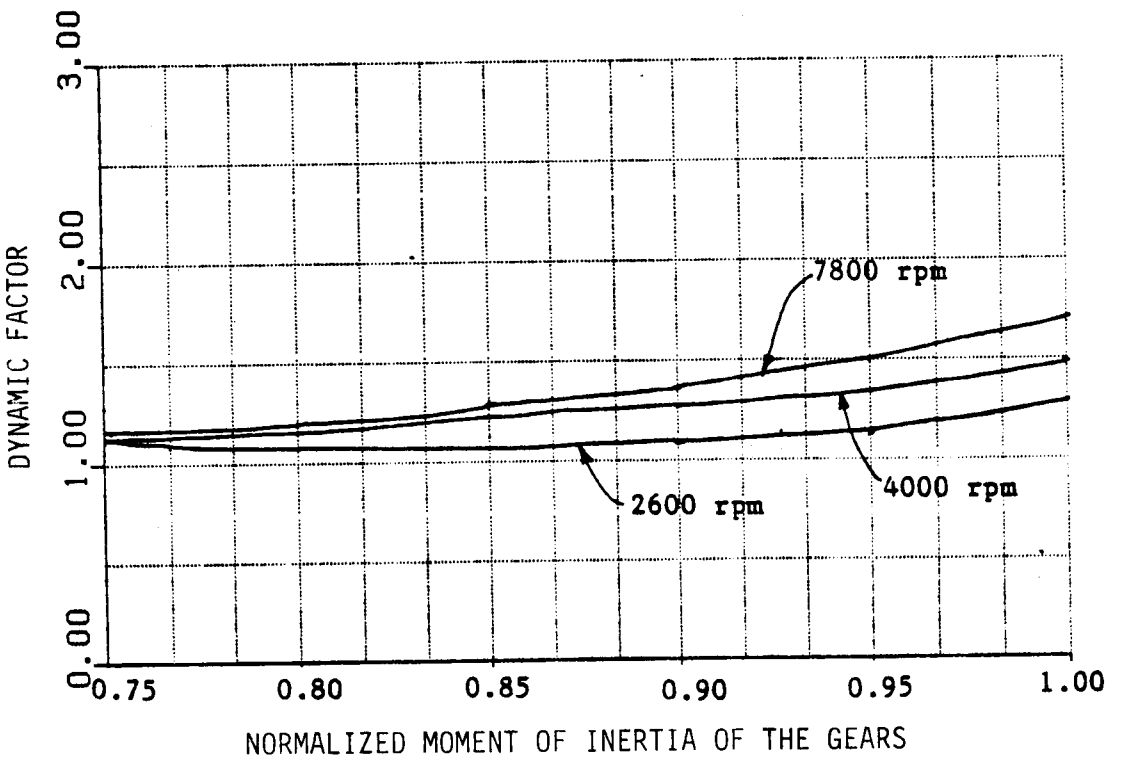

Figure III.10 Effect of Gear Inertia on the Dynamic Load Response

effect near the reasonance frequencies than at frequencies away from resonance.

III.3.4 Effect of Stiffness and Mass Moment of Inertia

A. Stiffness: Changes in shaft stiffness have a minor effect on the system dynamic response. However changes of tooth stiffness have a major effect on the response. Figure III.9 shows that the higher the tooth stiffness the lower the dynamic response. This is consistent with observations that as the tooth stiffness increases the mass effect of gear bodies on the system dynamics is reduced. Figure III.9 also shows that system resonance frequencies are increased as the tooth stiffness increases. This is a potentially useful effect for the design of gear systems.

B. Mass Moment of Inertia: The effect of the shaft masses is small compared to that of the gears. Figure III.10 shows that as the gear inertia is decreased the dynamic response is also decreased.

III.3.5 Effect of Diametral Pitch and Contact Ratio

For gears with different diametral pitches, the dynamic response is different due to the change in contact ratio. Gears with a finer pitch have a higher contact ratio. Since the contact ratio is a measure of the duration of the load being shared by more than one pair of teeth, it has a significant effect on the system dynamic response.

Figure III.11 shows a comparison between gears having different diametral pitches. The finer pitch gears, having a higher contact ratio, have a smaller dynamic load effect than the coarser pitch gears.

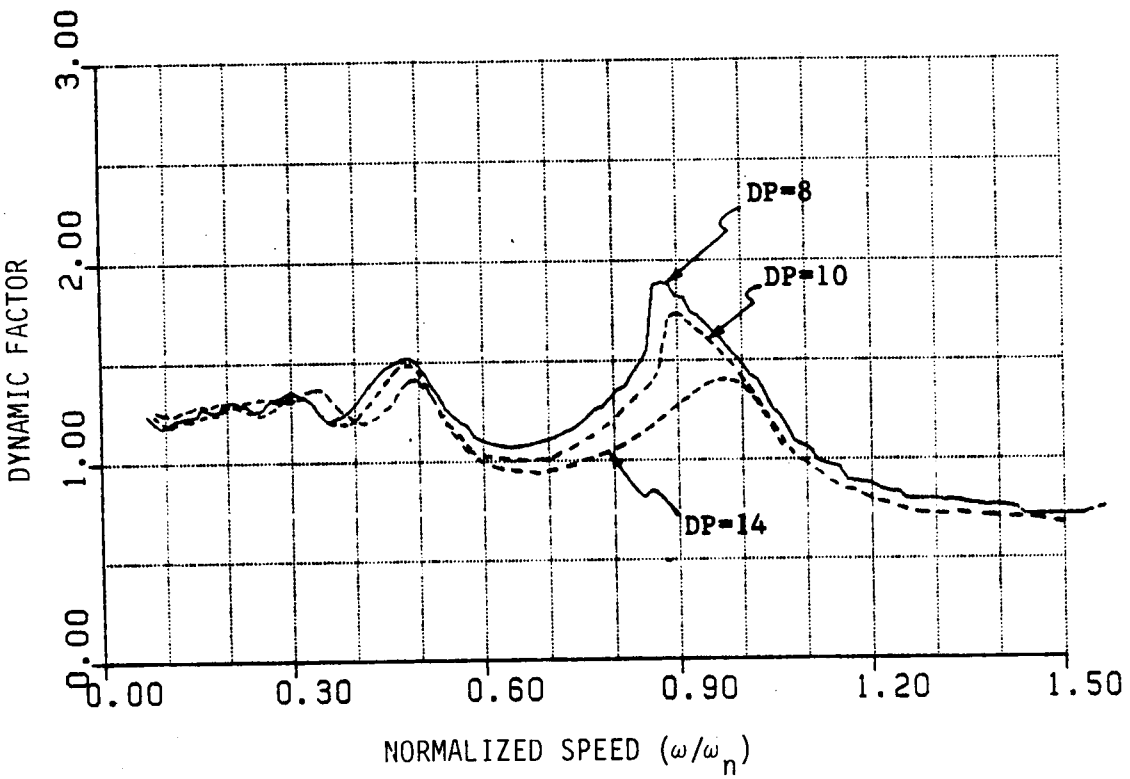

Figure III.11 Effect of Diametral Pitch on Dynamic Load Response

III.4 Comparison with Experimental and Empirical Data

At an American Gear Manufacturer's Association (AGMA) meeting in 1927 A. A. Ross [24] introduced the following empirical formula for the dynamic factor K_v:

$$K_v = \frac{78}{78 + \sqrt{v}} \qquad \text{(III.17)}$$

where v is the pitch line speed measured in ft/min. This expression came to receive acceptance as a standard factor used by the AGMA.

A similar factor for use with higher precision gears was introduced by Wellauer [25] in 1959:

$$K_v = \sqrt{\frac{78}{78 + \sqrt{v}}} \qquad \text{(III.18)}$$

Equation (III.17) and (III.18) are recognized as being conservative when applied with very high precision gears. That is they predict dynamic laods which are larger than the physical loads.

Buckingham [1] also developed an expression for the dynamic load in terms of the pitch line speed, the applied load and other geometrical and physical factors. Buckingham's formula is

$$W_d = W + [f_a(2f_2 - f_a]^{\frac{1}{2}} \qquad \text{(III.19)}$$

where W_d is the dynamic load, W is the applied load and the factors f_a and f_2 are

$$f_a = f_1 f_2/(f_1 + f_2) \qquad \text{(III.20)}$$

and

$$f_2 = FC + W \qquad \text{(III.21)}$$

where F is the face width in inches and C is a deformation factor given by:

$$C = 0.111\ e\ E_1 E_2/(E_1 + E_2) \qquad \text{(III.22)}$$

where e is a profile error factor and E_1 and E_2 are elastic contacts of the gears. The factor f, is

$$f_1 = 0.00025[(R_1 + R_2)/R_1 R_2]mV^2 \qquad \text{(III.23)}$$

where R_1 and R_2 are pitch radii of the gears, measured in inches, m is the effective mass of the gears and, as before, V is the pitch line speed in ft/min.

Finally, Kubo [26] has recorded results of extensive experimental studies on dynamic effects for high-precision spur gear systems.

Figure III.12 shows a comparison of the AGMA high-precision formula [Equation (III.18)], Buckingham's formula, Kubo's results, and the results of the computer simulation.

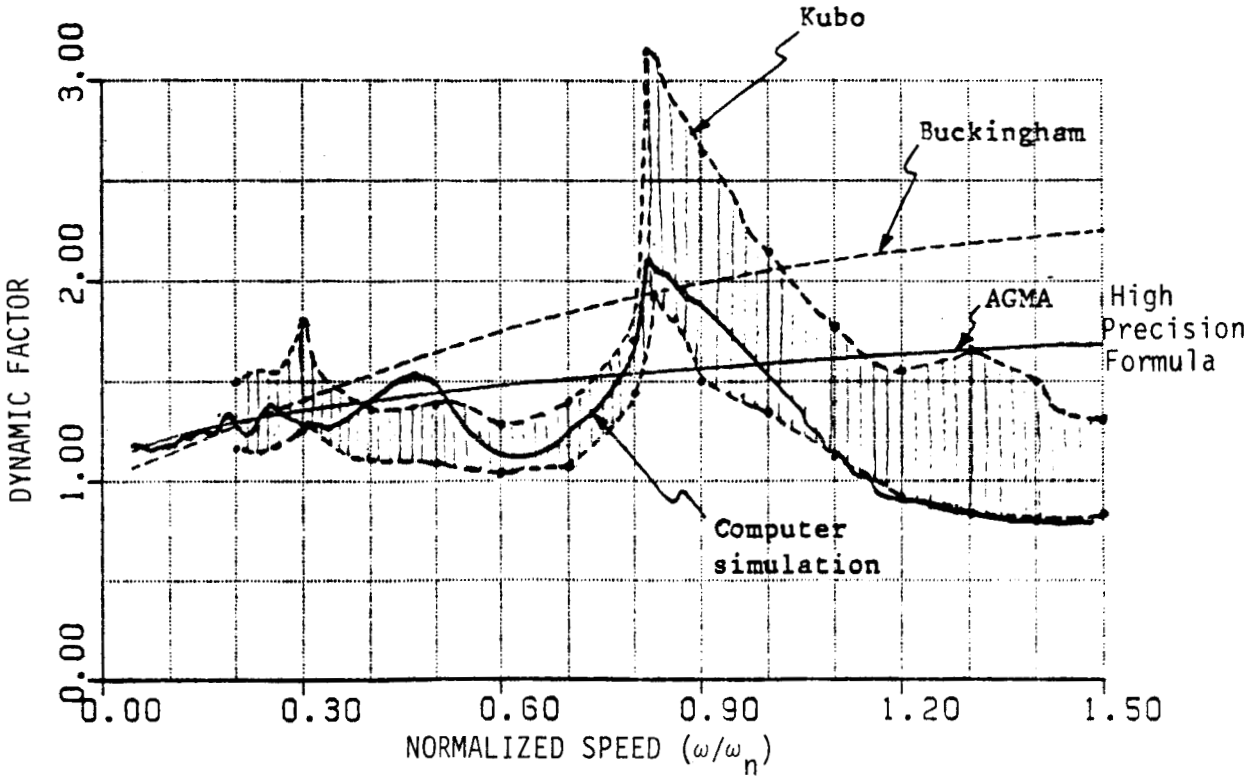

Figure III.12 Comparison of Experimental, Empirical, and Computer Simulation Results

IV. DISCUSSION

In reflecting upon the analysis there are several remarks which might summarize the findings:

1. The model of Figure II.2, Chapter 2 is relatively simple. Indeed, it consists of only two spur gears and two shafts. Still, many important aspects of dynamic loading are manifested by the model.

2. The model includes the effects of:

   a. Masses and movements of inertia of the gears and shafts.

   b. The stiffnesses of the gears and shafts.

   c. The operating speeds.

   d. The friction and damping.

   e. The tooth geometry.

3. The tooth stiffness is based upon a finite segment modelling. It is developed by using fundamental principles of mechanics of materials. It is dependent upon the tooth geometry--that is, the involute form.

4. The loading is found to be significantly affected by the contact ratio.

5. Tooth separation--leading to impact--occurs in the double contact region since the deflections are smallest in that region.

6. Dynamic load generally increases with operating speed until a system natural frequency is reached. The dynamic load decreases rapidly beyond the natural frequency.

7. The dynamic factor is largest for contact points near the tooth tip.

8. The applied load has a minor effect upon the dynamic factor. However, the dynamic factor decreases with applied load.

9. Damping and friction decrease the dynamic factor with the most dramatic effects occuring near the system natural frequencies.

10. Tooth stiffness has a significant effect upon the dynamic factor: The higher the stiffness, the lower the dynamic factor. Also, the greater the stiffness, the higher the rotating speed of peak response.

11. Shaft moment of inertia has a minimal effect upon the dynamic factor. However, the greater the inertia, the greater the dynamic effect.

12. Finally, for increased dimetral pitch, that is, high contact ratio gears, the dynamic factor will be decreased.

REFERERENCES

1. Lewis, W., "Investigations of the Strength of Gear Teeth," Proceedings of the Engineers Club of Philadelphia, 1893, pp. 16-23.

2. Buckingham, E., Analytical Mechanics of Gears, Dover Publication, Inc., New York, 1949.

3. Buckingham, E., "Dynamic Loads on Gear Teeth,"ASME Research Publication, New York, 1931.

4. Attia, A. Y., "Dynamic Loading of Spur Gear Teeth," ASME Trans., J. of Engrg. for Ind., Vol. 81, Ser. B. Feb. 1959, pp.1.

5. Nieman, G., and Rettig, H., "Error Induceed Dynamic Gear Tooth Loads," Proc. of Int'l Conf. on Gearing, 1958, pp. 31.

6. Harris, S. L., "Dynamic Loads on the Teeth of Spur Gears," Proc. Inst. Mech. Engr., Vol. 172, 1958, pp. 187.

7. Houser, D. R., and Seireg, A., "Evaluation of Dynamic Factors for Spur and Helical Gears," ASME Trans., J. Eng. for Ind., May 1970, pp. 504-515.

8. Ichimayu, K., and Hirano, I., "Dynamic Behavior of Heavy-Loaded Spur Gears," ASME Trans., J. Eng. for Ind., May 1974, pp. 373.

9. Cornell, R. W., and Westervelt, W. W., "Dynamic Tooth Loads and Stressing for High Contact Ratio Spur Gears," ASME Trans., J. Mech. Des., Vol. 100, Jan 1978.

10. Kasuba, R., and Evans, J. W., "An Extended Model for Determining Dynamic Loads in Spur Gearing," ASME Trans., J. Mech. Des., April 1981, pp. 398-409.

11. Wang, K. L., and Cheng, H. S., "A Numerical Solution to the Dynamic Load, Film Thickness, and Surface Temperature in Spur Gears," ASME Trans., J. Mech. Des., Jan 1981, pp. 177-187.

12. Nagaya, K., and Uematsu, S., "Effects of Moving Speeds of Dynamic Loads on the Deflection of Gear Teeth," ASME Trans., J. Mech. Des., April 1981, pp. 357-363.

13. Terauchi, Y., et. al., "On the Effects of Tooth Profile Modifications on the Dynamic Load and Sound Level of Spur Gears," Bulletin JSME, Sept. 1982, pp. 1474-1481.

14. Cornell, R. W., "Compliance and Stress Sensitivity of Spur Gear Teeth," ASME Trans., J. Mech. Des., April 1981.

15. Houser, D. A., and Tavalkoli, M. S., "Optimal Profile Modifications for the Minimization of Static Transmission Errors of Spur Gears," ASME Paper No. 84-DET-173, 1984.

16. Wang, S. M., "Static and Dynamic Response of Torsional Systems," Ph.D. Dissertation, University of Cincinnati, 1968.

17. Dowson, D., and Higginson, G. R., Elasto-Hydrodynamic Lubrication, Pergamon Press, N. Y., 1977.

18. Dareing, D. W., and Radzimovsky, E. I., "Lubricating Film Thickness and Load Capacity of Spur Gears: Analytical Investigation," ASME Paper No. 63-WA-85.

19. Akin, L. S., "EHD Lubricant Film Thickness Formulas for Power Transmission Gears," ASME Paper No. 73-Lub-21.

20. Trachman, E. G., "A Simplified Technique for Predicting Transaction in EHD Contacts," ASLE Trans., Vol. 21, No. 1, 1977, pp. 53-69.

21. Martin, K. F., "A Review of Friction Predictions in Gear Teeth," Wear, August 1978, pp. 201-238.

22. Benedict, G. H., and Kelley, B. W., "Instantaneous Coefficients of Gear Tooth Friction," ASLE Trans., Apr. 1961, pp. 59-70.

23. Anderson, N. E., and Loewenthal, S. H., "Spur Gear System Efficiency at Part and Full Load," NASA Tech. paper 1622, Feb. 1980.

24. Ross, A. A., "High-Speed Gears," Paper read at AGMA, 1927.

25. Wellauer, E. J., "An Analysis of Factors Used for Strength Rating Helical Gears," ASME Paper No. 59-A-121, 1959.

26. Dudly, D. W., Handbook of Practical Gear Design, McGraw Hill, New York, 1984, Chapter 9.

27. Nayfeh, A., and Mook, Nonlinear Oscillations, John Wiley & Sons, Inc., New York, 1979, Chapter 5.

28. Rogers, L. C., "Derivatives of Eigenvalues and Eigenvectors," AIAA Journal, May 1970, pp. 943-944.

29. Farshad, M., "Variations of Eigenvalues and Eigenfunctions in Continuum Mechanics," AIAA Journal, Apr. 1974, pp. 560-561.

30. Doughty, S., "Sensitivity of Torsional Natural Frequencies," ASME Trans., J. Eng. Ind., Feb. 1977, pp. 142-143.

31. Michalec, G. W., Precision Gearing: Theory and Practice, John Wiley & Sons, New York, 1966.

32. Smith, J. D., Gears and Their Vibration, Marcel Dekker, Inc., New York, 1983.

33. Tse, Morse, Hinkel, Mechanical Vibrations, 2nd Edition, Allyn and Bacon, Boston, 1978, pp. 231.

34. Furman, T. T., The Use of Computers in Engineering Design Van Nostrand Reinhold Co., New York, 1970, pp. 40-52.

35. Hahn, W. F., "Study of Instantaneous Load to Which Gear Teeth are Subjected," Ph.D. Dissertation, University of Illinois, 1969.

36. Heywood, R. B., Designing by Photoelasticity, Chapman and Hall, Ltd., 1952.

37. Lundberg, G., and Palmgren, A., "Dynamic Capacity of Rolling Bearings," Acta. Polytech. Mech. Eng. Sci., Vol. 1, No. 3, 1947.

1. Report No.	2. Government Accession No.	3. Recipient's Catalog No.
NASA CR-179473		

4. Title and Subtitle	5. Report Date
Dynamic Loading on Parallel Shaft Gears	July 1986
	6. Performing Organization Code

7. Author(s)	8. Performing Organization Report No.
MS 720124 Hsiang-Hsi (Edward) Lin and Ronald L. Huston	UC-MIE-051586-19
	10. Work Unit No.

9. Performing Organization Name and Address	11. Contract or Grant No.
University of Cincinnati Dept. of Mechanical and Industrial Engineering Cincinnati, Ohio 45221-0072 CP130085	NSG-3188
	13. Type of Report and Period Covered
12. Sponsoring Agency Name and Address	Contractor Report
National Aeronautics and Space Administration Washington, D.C. 20546	14. Sponsoring Agency Code
	505-62-51

15. Supplementary Notes

Final report. Project Managers: John J. Coy and Fred B. Oswald, Propulsion Systems Division, NASA Lewis Research Center, Cleveland, Ohio 44135. Hsiang-Hsi (Edward) Lin, Memphis State University, Dept. of Mechanical Engineering, Memphis, Tennessee 38152; Ronald L. Huston, University of Cincinnati, Dept. of Mechanical and Industrial Engineering, Cincinnati, Ohio 45221-0072.

16. Abstract

This report presents a computer-based analysis of the dynamic effects of spur gear systems. The method of analysis with its associated computer code is capable of determining the dynamic response of spur gear systems having involute tooth profiles and standard contact ratios. Various parameters affecting the system dynamic behavior are examined. Numerical results of the analysis are compared with semi-empirical formulae, AGME formulae, and experimental data. A close correlation with the experimental data is obtained.

17. Key Words (Suggested by Author(s))	18. Distribution Statement
Gear dynamics; Dynamic transmission loads; Transmission dynamics; Spur gear dynamics	Unclassified - unlimited STAR Category 37

19. Security Classif. (of this report)	20. Security Classif. (of this page)	21. No. of pages	22. Price*
Unclassified	Unclassified	79	A05

*For sale by the National Technical Information Service, Springfield, Virginia 22161